QCD equation of state with almost physical quark masses

M. Cheng,[1] N. H. Christ,[1] S. Datta,[2] J. van der Heide,[3] C. Jung,[4] F. Karsch,[3,4] O. Kaczmarek,[3] E. Laermann,[3] R. D. Mawhinney,[1] C. Miao,[3] P. Petreczky,[4,5] K. Petrov,[6] C. Schmidt,[4] W. Soeldner,[4] and T. Umeda[7]

[1]*Physics Department, Columbia University, New York, New York 10027, USA*
[2]*Department of Theoretical Physics, Tata Institute of Fundamental Research, Homi Bhabha Road, Mumbai 400005, India*
[3]*Fakultät für Physik, Universität Bielefeld, D-33615 Bielefeld, Germany*
[4]*Physics Department, Brookhaven National Laboratory, Upton, New York 11973, USA*
[5]*RIKEN-BNL Research Center, Brookhaven National Laboratory, Upton, New York 11973, USA*
[6]*Niels Bohr Institute, University of Copenhagen, Blegdamsvej 17, DK-2100 Copenhagen, Denmark*
[7]*Graduate School of Pure and Applied Sciences, University of Tsukuba, Tsukuba, Ibaraki 305-8571, Japan*
(Received 2 October 2007; published 22 January 2008)

We present results on the equation of state in QCD with two light quark flavors and a heavier strange quark. Calculations with improved staggered fermions have been performed on lattices with temporal extent $N_\tau = 4$ and 6 on a line of constant physics with almost physical quark mass values; the pion mass is about 220 MeV, and the strange quark mass is adjusted to its physical value. High statistics results on large lattices are obtained for bulk thermodynamic observables, i.e. pressure, energy and entropy density, at vanishing quark chemical potential for a wide range of temperatures, 140 MeV $\leq T \leq$ 800 MeV. We present a detailed discussion of finite cutoff effects which become particularly significant for temperatures larger than about twice the transition temperature. At these high temperatures we also performed calculations of the trace anomaly on lattices with temporal extent $N_\tau = 8$. Furthermore, we have performed an extensive analysis of zero temperature observables including the light and strange quark condensates and the static quark potential at zero temperature. These are used to set the temperature scale for thermodynamic observables and to calculate renormalized observables that are sensitive to deconfinement and chiral symmetry restoration and become order parameters in the infinite and zero quark mass limits, respectively.

DOI: 10.1103/PhysRevD.77.014511 PACS numbers: 11.15.Ha, 11.10.Wx, 12.38.Gc, 12.38.Mh

I. INTRODUCTION

Reaching a detailed understanding of bulk thermodynamics of QCD, e.g. the temperature dependence of pressure and energy density as well as the equation of state, $p(\epsilon)$ vs ϵ, is one of the central goals of nonperturbative studies of QCD on the lattice. The equation of state clearly is of central importance for the understanding of thermal properties of any thermodynamic system. It provides direct insight into the relevant degrees of freedom and their correlation in different phases of strongly interacting matter. We have some understanding of the equation of state in limiting cases of high and low temperatures from perturbation theory [1–5] and hadron gas phenomenology [6], respectively. In the transition region from the low temperature hadronic regime to the high temperature quark gluon plasma, however, one has to rely on a genuine nonperturbative approach, lattice regularized QCD, to study the nonperturbative properties of strongly interacting matter.

Lattice studies of bulk thermodynamics are particularly demanding as the most interesting observables, pressure and energy density, are given in terms of differences of dimension 4 operators. These differences are particularly difficult to evaluate because both terms being subtracted contain the pressure or energy density of the vacuum, an unphysical quantity that is approximately $1/(aT)^4$ larger than the sought-after difference. Numerical signals thus rapidly decrease with the fourth power of the lattice spacing, a, when one tries to approach the continuum limit at fixed temperature (T). For this reason improved actions, which allow one to perform calculations on rather coarse lattices with relatively small lattice discretization errors, are quite useful in thermodynamic calculations. Indeed, the early calculations of bulk thermodynamics with standard staggered [7] and Wilson [8] fermion discretization schemes have shown that at high temperature bulk thermodynamic observables are particularly sensitive to lattice discretization errors. This closely follows observations made in studies of the thermodynamics of $SU(3)$ gauge theories [9]. In order to minimize discretization errors at high temperature, improved staggered fermion actions—the p4-action [10] and the asqtad action [11]—have been used to study the QCD equation of state. Recent studies, performed with the asqtad action with almost physical quark mass values on lattices with two different values of the lattice cutoff [11], indeed show much smaller discretization errors than similar studies performed with the 1-link, stout smeared staggered fermion action [12]. Another source for cutoff errors arises, however, from the explicit breaking of flavor symmetry in the staggered fermion formulation. While this is not of much concern in the chirally symmetric high temperature phase of QCD, it leads to cutoff dependent modifications of the hadron spectrum and thus may influence the calculation of thermodynamic observables in the low temperature hadronic

phase of QCD. Techniques to reduce flavor symmetry breaking through the introduction of so-called "fat links" are thus generally exploited in numerical calculations with staggered fermions [13].

In this paper we report on a calculation of bulk thermodynamics in QCD with almost physical light quark masses and a physical value of the strange quark mass. Our calculations have been performed with a tree-level Symanzik-improved gauge action and an improved staggered fermion action, the p4-action with 3-link smearing (p4fat3), which removes $\mathcal{O}(a^2)$ cutoff effects at tree-level and also leads to small cutoff effects in $\mathcal{O}(g^2)$ perturbation theory [14]. At each temperature, we perform simulations with two degenerate light quark masses and a heavier strange quark mass for two different values of the lattice cutoff, corresponding to lattices with temporal extent $N_\tau = 4$ and 6. In these calculations we explore a wide range of temperatures varying from about 140 MeV to about 800 MeV. This corresponds to the temperature interval relevant for current experimental studies of dense matter in heavy ion collisions at RHIC as well as the forthcoming experiments at the CERN LHC. Bare quark masses have been adjusted to keep physical masses approximately constant when the lattice cutoff is varied. At high temperatures, $T \gtrsim 350$ MeV, we also performed calculations on lattices with temporal extent $N_\tau = 8$ to get control over cutoff effects in the high temperature limit.

We will start in the next section by reviewing basic thermodynamic relations in the continuum valid for thermodynamic calculations on such *lines of constant physics* (LCP). In Sec. III we outline details of our calculational setup with improved staggered fermions. In Sec. IV we present our zero temperature calculations needed to define the line of constant physics and the temperature scale deduced from properties of the static quark-antiquark potential. Section V is devoted to the presentation of our basic result, the difference between energy density and 3 times the pressure from which we obtain all other thermodynamic observables, e.g. the pressure, energy and entropy densities as well as the velocity of sound. Section VI is devoted to a discussion of the temperature dependence of Polyakov loop expectation values and chiral condensates which provides a comparison between the deconfining and chiral symmetry restoring features of the QCD transition. We finally present a discussion of our results and a comparison with other improved staggered fermion calculations of bulk thermodynamics in Sec. VII.

II. THERMODYNAMICS ON LINES OF CONSTANT PHYSICS

To start our discussion of QCD thermodynamics on the lattice we recall some basic thermodynamic relations in the continuum. For large, homogeneous media the basic bulk thermodynamic observables we will consider here can be obtained from the grand canonical partition function with vanishing quark chemical potentials, $Z(T, V)$. We introduce the grand canonical potential, $\Omega(T, V)$, normalized such that it vanishes at vanishing temperature,

$$\Omega(T, V) = T \ln Z(T, V) - \Omega_0, \tag{1}$$

with $\Omega_0 = \lim_{T\to 0} T \ln Z(T, V)$. With this we obtain the thermal part of the pressure (p) and energy density (ϵ)

$$p = \frac{1}{V}\Omega(T, V), \qquad \epsilon = \frac{T^2}{V}\frac{\partial \Omega(T, V)/T}{\partial T}, \tag{2}$$

which by construction both vanish at vanishing temperature. Using these relations one can express the difference between ϵ and $3p$, i.e. the thermal contribution to the trace of the energy-momentum tensor $\Theta^{\mu\mu}(T)$, in terms of a derivative of the pressure with respect to temperature, i.e.

$$\frac{\Theta^{\mu\mu}(T)}{T^4} \equiv \frac{\epsilon - 3p}{T^4} = T\frac{\partial}{\partial T}(p/T^4). \tag{3}$$

In fact, it is $\Theta^{\mu\mu}(T)$ which is the basic thermodynamic quantity conveniently calculated on the lattice. All other bulk thermodynamic observables, e.g. p/T^4, ϵ/T^4 as well as the entropy density, $s/T^3 \equiv (\epsilon + p)/T^4$, can be deduced from this using the above thermodynamic relations. In particular, we obtain the pressure from $\Theta^{\mu\mu}(T)$ through integration of Eq. (3),

$$\frac{p(T)}{T^4} - \frac{p(T_0)}{T_0^4} = \int_{T_0}^{T} \mathrm{d}T' \frac{1}{T'^5}\Theta^{\mu\mu}(T'). \tag{4}$$

Usually, the temperature for the lower integration limit, T_0, is chosen to be a temperature sufficiently deep in the hadronic phase of QCD where the pressure, $p(T_0)$, receives contributions only from massive hadronic states and is already exponentially small. We will discuss this in more detail in Sec. V. Equation (4) then directly gives the pressure at temperature T. Using p/T^4 determined from Eq. (4) and combining it with Eq. (3), we obtain ϵ/T^4 as well as s/T^3. This makes it evident that there is indeed only one independent bulk thermodynamic observable calculated in the thermodynamic (large volume) limit. All other observables are derived through standard thermodynamic relations so that thermodynamic consistency of all bulk thermodynamic observables is insured by construction.

We stress that the normalization introduced here for the grand canonical potential, Eq. (1), forces the pressure and energy density to vanish at $T = 0$. As a consequence of this normalization, any nonperturbative structure of the QCD vacuum, e.g. quark and gluon condensates, that contribute to the trace anomaly $\Theta^{\mu\mu}(0)$, and would lead to a non-vanishing vacuum pressure and/or energy density, eventually will show up as nonperturbative contributions to the high temperature part of these thermodynamic observables. This is similar to the normalization used, e.g. in the bag model and the hadron resonance gas, but differs from the normalization used, e.g. in resummed perturbative calculation at high temperature [15,16] or phenomenologi-

cal (quasiparticle) models for the high temperature phase of QCD [17]. This should be kept in mind when comparing results for the equation of state (EOS) with perturbative and model calculations. We also note that ambiguities in normalizing pressure and energy density at zero temperature drop out in a calculation of the entropy density which thus is the preferred observable for such comparisons.

III. LATTICE FORMULATION

In a lattice calculation, temperature and volume are given in terms of the temporal (N_τ) and spatial (N_σ) lattice extent as well as the lattice spacing, a, which is controlled through the lattice gauge coupling $\beta \equiv 6/g^2$,

$$T = \frac{1}{N_\tau a(\beta)}, \qquad V = (N_\sigma a(\beta))^3. \tag{5}$$

As all observables that are calculated on the lattice are functions of the coupling, β, we may rewrite Eq. (3) in terms of a derivative taken with respect to β rather than T. Furthermore we adopt the normalization of the pressure as introduced in Eq. (1). This insures a proper renormalization of thermodynamic quantities and, as a consequence, forces the pressure to vanish in the vacuum, i.e. at $T = 0$.

Let us write the QCD partition function on a lattice of size $N_\sigma^3 N_\tau$ as

$$Z_{\rm LCP}(\beta, N_\sigma, N_\tau) = \int \prod_{x,\mu} {\rm d}U_{x,\mu} {\rm e}^{-S(U)}, \tag{6}$$

where $U_{x,\mu} \in SU(3)$ denotes the gauge link variables and $S(U) = \beta S_G(U) - S_F(U, \beta)$ is the Euclidean action, which is composed out of a purely gluonic contribution, $S_G(U)$, and the fermionic part, $S_F(U, \beta)$, which arises after integration over the fermion fields. We will specify this action in more detail in the next section but note here that we will use tree-level improved gauge and fermion actions. Although it would be straightforward to introduce one-loop or tadpole improvement factors in the action the setup used here greatly simplifies the analysis of thermodynamic observables and in some cases also gives a more direct relation to corresponding observables in the continuum.

When using only tree-level improvement the gluonic action does not depend on the gauge coupling, β, and the fermion action depends on β only through the bare light ($\hat{m}_l$) and strange ($\hat{m}_s$) quark masses. The subscript LCP in Eq. (6) indicates that we have defined the partition function $Z_{\rm LCP}$ on a line of constant physics, i.e. when approaching the continuum limit by increasing the gauge coupling ($\beta \to \infty$) the bare quark masses ($\hat{m}_l(\beta), \hat{m}_s(\beta)$) in the QCD Lagrangian are tuned towards zero such that the vacuum properties of QCD remain unchanged. The quark masses thus are not independent parameters but are functions of β which are determined through constraints imposed on zero temperature observables; e.g. one demands that a set of hadron masses remains unchanged when the continuum limit is approached on a LCP.

We now may rewrite Eq. (3) in terms of observables calculable in lattice calculations at zero and nonzero temperature,

$$\frac{\Theta^{\mu\mu}(T)}{T^4} = -R_\beta(\beta) N_\tau^4 \left(\frac{1}{N_\sigma^3 N_\tau} \left\langle \frac{{\rm d}S}{{\rm d}\beta} \right\rangle_\tau - \frac{1}{N_\sigma^3 N_0} \left\langle \frac{{\rm d}S}{{\rm d}\beta} \right\rangle_0 \right). \tag{7}$$

Here $\langle \ldots \rangle_x$, with $x = \tau, 0$ denote expectation values evaluated on finite temperature lattices of size $N_\sigma^3 N_\tau$, with $N_\tau \ll N_\sigma$, and zero temperature lattices, i.e. on lattices with large temporal extent, $N_\sigma^3 N_\tau$ with $N_\tau \equiv N_0 \gtrsim N_\sigma$, respectively. Furthermore, R_β denotes the lattice version of the QCD β-function which arises as a multiplicative factor in the definition of $\Theta^{\mu\mu}(T)$ because derivatives with respect to T have been converted to derivatives with respect to the lattice spacing a on lattices with fixed temporal extent N_τ,

$$R_\beta(\beta) \equiv T \frac{{\rm d}\beta}{{\rm d}T} = -a \frac{{\rm d}\beta}{{\rm d}a}. \tag{8}$$

We note that in the weak coupling, large β limit, R_β approaches the universal form of the 2-loop β-function of 3-flavor QCD,

$$R_\beta(\beta) = 12 b_0 + 72 b_1/\beta + \mathcal{O}(\beta^{-2}), \tag{9}$$

with $b_0 = 9/16\pi^2$ and $b_1 = 1/4\pi^4$.

We analyze the thermodynamics of QCD with two degenerate light quarks ($\hat{m}_l \equiv \hat{m}_u = \hat{m}_d$) and a heavier strange quark ($\hat{m}_s$) described by the QCD partition function given in Eq. (6). For our studies of bulk thermodynamics we use the same discretization scheme which has been used recently by us in the study of the QCD transition temperature [18], i.e. we use an $\mathcal{O}(a^2)$ tree-level improved gauge action constructed from a 4-link plaquette term and a planar 6-link Wilson loop as well as a staggered fermion action that contains a smeared 1-link term and bent 3-link terms. We call this action the p4fat3-action; further details are given in Ref. [10] where the p4fat3 action was first used in studies of the QCD equation of state on lattices with temporal extent $N_\tau = 4$ and larger quark masses. With this action, bulk thermodynamic quantities like pressure and energy density are $\mathcal{O}(a^2)$ tree-level improved; corrections to the high temperature ideal gas limit only start at $\mathcal{O}(1/N_\tau^4)$ and are significantly smaller than for the Naik action or the standard staggered action which suffers from large $\mathcal{O}(1/N_\tau^2)$ cutoff effects at high temperature. An analysis of cutoff effects in the ideal gas limit and in $\mathcal{O}(g^2)$ lattice perturbation theory [14] shows that deviations from perturbative results are already only a few percent for lattices with temporal extent as small as $N_\tau = 6$.

Following the notation used in Ref. [18] the Euclidean action is given as

$$S(U) = \beta S_G(U) - S_F(U, \beta), \tag{10}$$

with a gluonic contribution, $S_G(U)$, and a fermionic part, $S_F(U, \beta)$. The latter can be expressed in terms of the staggered fermion matrices, $D_{\hat{m}_l(\hat{m}_s)}$, for two light ($\hat{m}_l$) and a heavier strange quark ($\hat{m}_s$),

$$S_F(U, \beta) = \frac{1}{2} \mathrm{Tr} \ln D(\hat{m}_l(\beta)) + \frac{1}{4} \mathrm{Tr} \ln D(\hat{m}_s(\beta)). \tag{11}$$

Here we took the fourth root of the staggered fermion determinant to represent the contribution of a single fermion flavor to the QCD partition function.[1]

We also introduce the light and strange quark condensates calculated at finite ($x = \tau$) and zero temperature ($x = 0$), respectively,

$$\langle \bar{\psi}\psi \rangle_{q,x} \equiv \frac{1}{4} \frac{1}{N_\sigma^3 N_x} \langle \mathrm{Tr} D^{-1}(\hat{m}_q) \rangle_x, \qquad q = l, s, \qquad x = 0, \tau, \tag{12}$$

as well as expectation values of the gluonic action density,

$$\langle s_G \rangle_x \equiv \frac{1}{N_\sigma^3 N_x} \langle S_G \rangle_x. \tag{13}$$

All numerical calculations have been performed using the rational hybrid Monte Carlo (RHMC) algorithm [22] with parameters that have been optimized [18] to reach acceptance rates of about 70%. Some details on our tuning of parameters of the RHMC algorithm have been given in [23].

For the discussion of the thermodynamics on a LCP it sometimes is convenient to parametrize the quark mass dependence of S_F in terms of the light quark mass $\hat{m}_l$ and the ratio $h \equiv \hat{m}_s/\hat{m}_l$ rather than $\hat{m}_l$ and $\hat{m}_s$ separately. We thus write the β-dependence of the strange quark mass as $\hat{m}_s(\beta) = \hat{m}_l(\beta) h(\beta)$. In the evaluation of $(\epsilon - 3p)/T^4$ we then will need to know the derivatives of these parametrizations with respect to β. We define

$$R_m(\beta) = \frac{1}{\hat{m}_l(\beta)} \frac{\mathrm{d}\hat{m}_l(\beta)}{\mathrm{d}\beta}, \qquad R_h(\beta) = \frac{1}{h(\beta)} \frac{\mathrm{d}h(\beta)}{\mathrm{d}\beta}. \tag{14}$$

With these definitions we may rewrite Eq. (7) as

$$\frac{\epsilon - 3p}{T^4} = T \frac{\mathrm{d}}{\mathrm{d}T} \left(\frac{p}{T^4} \right) = R_\beta(\beta) \frac{\partial p/T^4}{\partial \beta} = \frac{\Theta_G^{\mu\mu}(T)}{T^4} + \frac{\Theta_F^{\mu\mu}(T)}{T^4} + \frac{\Theta_h^{\mu\mu}(T)}{T^4}, \tag{15}$$

with

$$\frac{\Theta_G^{\mu\mu}(T)}{T^4} = R_\beta [\langle s_G \rangle_0 - \langle s_G \rangle_\tau] N_\tau^4, \tag{16}$$

$$\frac{\Theta_F^{\mu\mu}(T)}{T^4} = -R_\beta R_m [2\hat{m}_l (\langle \bar{\psi}\psi \rangle_{l,0} - \langle \bar{\psi}\psi \rangle_{l,\tau}) + \hat{m}_s (\langle \bar{\psi}\psi \rangle_{s,0} - \langle \bar{\psi}\psi \rangle_{s,\tau})] N_\tau^4, \tag{17}$$

$$\frac{\Theta_h^{\mu\mu}(T)}{T^4} = -R_\beta R_h \hat{m}_s [\langle \bar{\psi}\psi \rangle_{s,0} - \langle \bar{\psi}\psi \rangle_{s,\tau}] N_\tau^4. \tag{18}$$

We will show in the next section that to a good approximation $h(\beta)$ stays constant on a LCP. R_h thus vanishes on the LCP and consequently the last term in Eq. (15), $\Theta_h^{\mu\mu}$, will not contribute to the thermal part of the trace anomaly, $\Theta^{\mu\mu}(T)$. The other two terms stay finite in the continuum limit and correspond to the contribution of the thermal parts of gluon and quark condensates to the trace anomaly. We note that the latter contribution vanishes in the chiral limit of three flavor QCD ($\hat{m}_l, \hat{m}_s \to 0$). The trace anomaly would then entirely be given by $\Theta_G^{\mu\mu}(T)$ and the observables entering the calculation of bulk thermodynamic quantities in the chiral limit of QCD would reduce to those needed also in a pure $SU(3)$ gauge theory [9]. In fact, we also find that for physical values of the quark masses the trace anomaly is dominated by the gluonic contribution, $\Theta_G^{\mu\mu}(T)$. As will become clear in Sec. V $\Theta_F^{\mu\mu}(T)$ contributes less than 10% to the total trace anomaly for temperatures large than about twice the transition temperature.

We also note that the prefactor in Eq. (17) will approach unity in the continuum limit as R_m attains a universal form up to 2-loop level which is similar to that of R_β^{-1} and is only modified through the anomalous dimension of the quark mass renormalization [24]. For the relevant combination of β-functions that enters the fermionic part of the trace anomaly, one has

$$-(R_\beta(\beta) R_m(\beta))^{1-\mathrm{loop}} = 1 + \frac{16 b_0}{3\beta}. \tag{19}$$

IV. STATIC QUARK POTENTIAL AND THE LINE OF CONSTANT PHYSICS

A. Construction of the line of constant physics

We will calculate thermodynamic observables on a LCP that is defined at $T = 0$ as a line in the space of light and strange bare quark masses parametrized by the gauge coupling β. Each point on this line corresponds to identical physical conditions at different values of the lattice cutoff which is tuned towards the continuum limit by increasing the gauge coupling β. We define the line of constant physics by demanding (i) that the ratio of masses for the strange pseudoscalar and the kaon mass, $m_{\bar{s}s}/m_K$, stays constant and (ii) that $m_{\bar{s}s}$ expressed in units of the scale parameter r_0 stays constant. The latter gives the distance at which the slope of the zero temperature, static quark

[1] There is a controversy regarding the validity of the rooting approach in numerical calculations with staggered fermions. For further details we refer to recent reviews presented at the Lattice conference [19–21] and references therein.

potential, $V_{\bar{q}q}(r)$, attains a certain value. We also introduce the scale r_1, which frequently is used on finer lattices to convert lattice results expressed in units of the cutoff to physical scales,

$$\left(r^2\frac{\mathrm{d}V_{\bar{q}q}(r)}{\mathrm{d}r}\right)_{r=r_0} = 1.65, \qquad \left(r^2\frac{\mathrm{d}V_{\bar{q}q}(r)}{\mathrm{d}r}\right)_{r=r_1} = 1.0. \tag{20}$$

We checked that (i) and (ii) also hold true, if we replace $m_{\bar{s}s}$ by the mass of the light quark pseudoscalar meson, m_π. However, errors on $m_\pi r_0$ and (m_π/m_K) are generally larger which, in particular, at large values of β makes the parametrization of the LCP less stringent.

Leading order chiral perturbation theory suggests that the ratio $(m_{\bar{s}s}/m_K)^2$ is proportional to $\hat{m}_s/(\hat{m}_l + \hat{m}_s)$. One thus expects this ratio to stay constant for fixed $h = \hat{m}_s/\hat{m}_l$. This is, indeed fulfilled in the entire regime of couplings, β, explored in our calculations (see Table I). The first condition for fixing the LCP parameters thus, in practice, has been replaced by choosing $h = \hat{m}_l/\hat{m}_s$ to be constant. As a consequence we find $R_h(\beta) = 0$, which simplifies the calculation of thermodynamic quantities.

In order to define a line of constant strange quark mass, as a second condition for the LCP we demand that the product $m_{\bar{s}s}r_0$ stays constant. For our LCP we chose 1.59 as the value for the product. Here one should note that $m_{\bar{s}s}$ determined in our calculations only receives contributions from connected diagrams and does not include disconnected loops. In order to compare our value (1.59, see discussion below) to a physical one, we therefore follow the argumentation of Ref. [25] and adopt $m_{\bar{s}s} = \sqrt{2m_K^2 - m_\pi^2} = 686$ MeV as the physical mass of our strange pseudoscalar. Together with the scale $r_0 = 0.469(7)$ fm as determined in Ref. [26] through a comparison of r_0 with level splittings of the charmonium system [27], this yields $m_{\bar{s}s}r_0 \simeq 1.63$. Of course, there is some ambiguity in this choice as current determinations of r_0 differ by about 10% [26,28]. This introduces some systematic error in the definition of the *physical LCP*. The main reason for deviation from the physical LCP in the present calculation, however, is due to the choice of the light quark masses which are about a factor two too large.

Fixing the light and strange pseudoscalar masses in units of r_0 required some trial runs for several β values. We then used the leading order chiral perturbation theory *Ansatz* $m_{\bar{s}s}^2 \sim \hat{m}_s$ (or $m_\pi^2 \sim \hat{m}_l$) to choose $\hat{m}_s$ and $\hat{m}_l \equiv \hat{m}_s/10$ at several values of the gauge coupling and used a renormalization group inspired interpolation to determine quark mass values at several other β values at which high statistics simulations have been performed. It turned out that these values are best fitted by $m_{\bar{s}s}r_0 = 1.59$. We thus use this value rather than the value 1.63 mentioned above, to define our LCP. For all other simulations we then used the results of these zero temperature calculations to determine the quark mass values that belong to a line of constant physics characterized by

$$\text{LCP}: \quad (i)\ m_{\bar{s}s}r_0 = 1.59, \quad (ii)\ h \equiv \hat{m}_s/\hat{m}_l = 10.$$

In general our calculations are thus performed at parameter values close to the LCP which is defined by the above condition. The parameters of all our zero temperature calculations performed to determine the LCP, results for meson masses and parameters of the static quark potential are summarized in Table I. As can be seen, at our actual simulation points the results for $m_{\bar{s}s}r_0$ fluctuate around the mean value by a few percent. We also checked the sensitivity of the meson masses used to determine the LCP to finite volume effects. At $\beta = 3.49$ and 3.54 we performed calculations on 32^4 lattices in addition to the $16^3 \cdot 32$ lattices. As can bee seen from Table I results for $m_{\bar{s}s}$ and m_K agree within statistical errors and volume effects are at most on the level of 2% for the light pseudoscalar.

The LCP is furthermore characterized by $m_\pi/m_K = 0.435(2)$ and $m_{\bar{s}s}/m_K = 1.33(1)$. Using $r_0 = 0.469(7)$ fm to convert to physical scales we find that on the LCP the light and strange pseudoscalar masses are $m_\pi \simeq 220(4)$ MeV, $m_{\bar{s}s} \simeq 669(10)$ MeV and the kaon mass is given by $m_K \simeq 503(6)$ MeV.

B. The static quark potential and the scale r_0

On the LCP we determine several parameters, e.g. the short distance scale r_0 and the linear slope parameter, the string tension σ, that characterize the shape of the static quark potential calculated at $T = 0$ in a fixed range of physical distances. The distance r_0, defined in Eq. (20), is used to define the temperature scale for the thermodynamics calculations.

The static quark potential, $V_{\bar{q}q}(r)$, has been calculated from smeared Wilson loops as described in [18] for all parameter sets listed in Table I. We checked that the smeared Wilson loops project well onto the ground state at all values of the cutoff by verifying the independence of the extracted potential parameters on the number of smearing levels used in the analysis. The set of gauge couplings, $\beta \in [3.15, 4.08]$, used in this analysis covers a large interval in which the lattice cutoff changes by a factor 6 from $a \simeq 0.3$ fm down to $a \simeq 0.05$ fm. When analyzing the static potential over such a wide range of cutoff values one should make sure that the potential is analyzed in approximately the same range of physical distances. The fit interval $[(r/a)_{\text{min}}, (r/a)_{\text{max}}]$ for fits with a Cornell type *Ansatz* for the static potential thus has been adjusted for the different values of gauge couplings such that it covers approximately the same range of physical distances, $r_0/2 \lesssim r \lesssim 2r_0$, or $0.25\ \text{fm} \lesssim r \lesssim 1$ fm. We confirmed our analysis of the static quark potential and the determination of r_0 also independently by using spline interpolations which are not biased by a particular *Ansatz* for the form of the potential.

TABLE I. Light quark and strange pseudoscalar meson masses and parameters of the static quark potential calculated on zero temperature lattices of size $N_\sigma^3 N_\tau$. The last column gives the renormalization constants times r_0 needed to renormalize the heavy quark potential to the string potential at distance $r/r_0 = 1.5$.

β	$100\hat{m}_l$	$N_\sigma^3 \cdot N_\tau$	$m_\pi a$	$m_{\bar{s}s} a$	$m_K a$	r_0/a	$\sqrt{\sigma} a$	$c(g^2) r_0$
3.150	1.100	$16^3 \cdot 32$	0.3410(2)	1.0474(1)	0.7854(2)	1.467(72)	0.75(18)	0.97(12)
3.210	1.000	$16^3 \cdot 32$	0.3262(1)	0.9988(1)	0.7496(1)	1.583(36)	0.685(75)	1.118(68)
3.240	0.900	$16^3 \cdot 32$	0.3099(2)	0.9485(2)	0.7125(3)	1.669(31)	0.658(36)	1.243(67)
3.277	0.765	$16^3 \cdot 32$	0.2881(7)	0.8769(5)	0.6599(6)	1.797(19)	0.612(53)	1.362(53)
3.290	0.650	$16^3 \cdot 32$	0.2667(8)	0.8104(7)	0.6101(8)	1.823(16)	0.623(32)	1.362(29)
3.335	0.620	$16^3 \cdot 32$	0.2594(3)	0.7884(2)	0.5941(5)	1.995(11)	0.5668(73)	1.504(22)
3.351	0.591	$16^3 \cdot 32$	0.2541(7)	0.7692(5)	0.5800(7)	2.069(12)	0.551(11)	1.594(24)
3.382	0.520	$16^3 \cdot 32$	0.2370(6)	0.7194(5)	0.5422(5)	2.230(14)	0.5100(82)	1.718(57)
3.410	0.412	$16^3 \cdot 32$	0.2098(4)	0.6371(6)	0.4796(8)	2.503(18)	0.440(10)	2.073(49)
3.420	0.390	$24^3 \cdot 32$	0.2029(8)	0.6177(5)	0.4675(5)	2.577(11)	0.4313(56)	2.124(33)
3.430	0.370	$24^3 \cdot 32$	0.1986(6)	0.6000(3)	0.4529(5)	2.6467(81)	0.4225(53)	2.178(17)
3.445	0.344	$24^3 \cdot 32$	0.1909(7)	0.5749(4)	0.4335(5)	2.813(15)	0.3951(68)	2.388(35)
3.455	0.329	$24^3 \cdot 32$	0.1833(10)	0.5580(6)	0.4204(8)	2.856(20)	0.3895(68)	2.375(42)
3.460	0.313	$16^3 \cdot 32$	0.1808(16)	0.5443(11)	0.4102(11)	2.890(16)	0.3831(84)	2.391(55)
3.470	0.295	$24^3 \cdot 32$	0.1686(19)	0.5233(8)	0.3940(12)	3.065(18)	0.3592(75)	2.617(41)
3.490	0.290	$16^3 \cdot 32$	0.1689(14)	0.5115(11)	0.3842(11)	3.223(31)	0.3423(66)	2.757(59)
3.490	0.290	32^4	0.1679(8)	0.5113(8)	0.3840(7)			
3.510	0.259	$16^3 \cdot 32$	0.1525(40)	0.4740(20)	0.3554(22)	3.423(61)	0.322(14)	2.934(92)
3.540	0.240	$16^3 \cdot 32$	0.1495(24)	0.4458(20)	0.3358(19)	3.687(34)	0.3011(46)	3.128(51)
3.540	0.240	32^4	0.1469(11)	0.4451(6)	0.3339(11)			
3.570	0.212	$24^3 \cdot 32$	0.1347(53)	0.4053(18)	0.3028(23)	4.009(26)	0.2743(38)	3.414(47)
3.630	0.170	$24^3 \cdot 32$	0.1126(20)	0.3386(7)	0.2537(8)	4.651(41)	0.2352(44)	3.939(59)
3.690	0.150	$24^3 \cdot 32$	0.1020(90)	0.2960(20)	0.2230(30)	5.201(48)	0.2116(36)	4.320(63)
3.760	0.130	$24^2 \cdot 32 \cdot 48$	0.0857(32)	0.2530(16)	0.1894(16)	6.050(61)	0.1810(29)	4.984(73)
3.820	0.125	$32^3 \cdot 32$	0.0830(40)	0.2310(38)	0.1744(50)	6.835(44)	0.1701(21)	5.541(106)
3.920	0.110	$32^3 \cdot 32$	0.0750(70)	0.2020(10)	0.1550(20)	7.814(83)	0.1423(24)	6.037(72)
4.080	0.081	$32^3 \cdot 32$	0.0700(70)	0.1567(36)	0.1220(50)	10.39(23)	0.1060(35)	7.710(183)

The left-hand part of Fig. 1 shows the static quark potential for several of our parameter sets. We have renormalized these potentials by matching[2] all potentials at a large distance, $r/r_0 = 1.5$, to a common value that is taken to be identical to the large distance string potential, $V_{\text{string}}(r) = -\pi/12r + \sigma r$. The result of this matching is shown in the lower part of Fig. 1(left) and the constant shifts needed to obtain these renormalized potentials are listed in Table I. The good matching of all the potential data obtained at different values of the cutoff already gives a good idea of the smallness of finite cutoff effects in this observable. We note that this matching procedure provides renormalization constants for the static quark potential, which we also will use later to renormalize the Polyakov loop expectation value.

To further analyze the shape of the static quark potential we determined the scale parameter r_0/a as well as the square root of the string tension in lattice units, $\sqrt{\sigma}a$. These parameters have been obtained from three and four parameter fits. As described in [18] the latter fit *Ansatz* has been used to estimate systematic errors in our analysis of the scale parameters.

Results for r_0/a and $\sqrt{\sigma}a$ are given in Table I. We note that the product $r_0\sqrt{\sigma}$ stays constant on the LCP and changes by less than 2% in the entire range of couplings β in which the lattice cutoff changes by a factor 6. For $a \leq 0.15$ fm we used a quadratic fit *Ansatz*, $(r_0\sqrt{\sigma})_a = r_0\sqrt{\sigma} + c(a/r_0)^2$, to fit 10 data points. The asymptotic value for $r_0\sqrt{\sigma}$ coincides within errors with a simple average over all values of $(r_0\sqrt{\sigma})_a$ in this interval. This confirms that $\mathcal{O}(a^2)$ corrections indeed are small for this product. Similarly we determined the scale parameter r_1 frequently used to set the scale in calculations performed on finer lattices. Both fits for $r_0\sqrt{\sigma}$ and r_0/r_1 yield $\chi^2/dof \simeq 0.7$. From this analysis we obtain the parameters characterizing the shape of the heavy quark potential at masses in the vicinity of the LCP,

$$r_0\sqrt{\sigma} = 1.1034(40), \qquad r_0/r_1 = 1.4636(60). \tag{21}$$

[2]Further details on the matching of the zero temperature heavy quark potentials, its application to the renormalization of the Polyakov loop and finite temperature free energies will be published elsewhere.

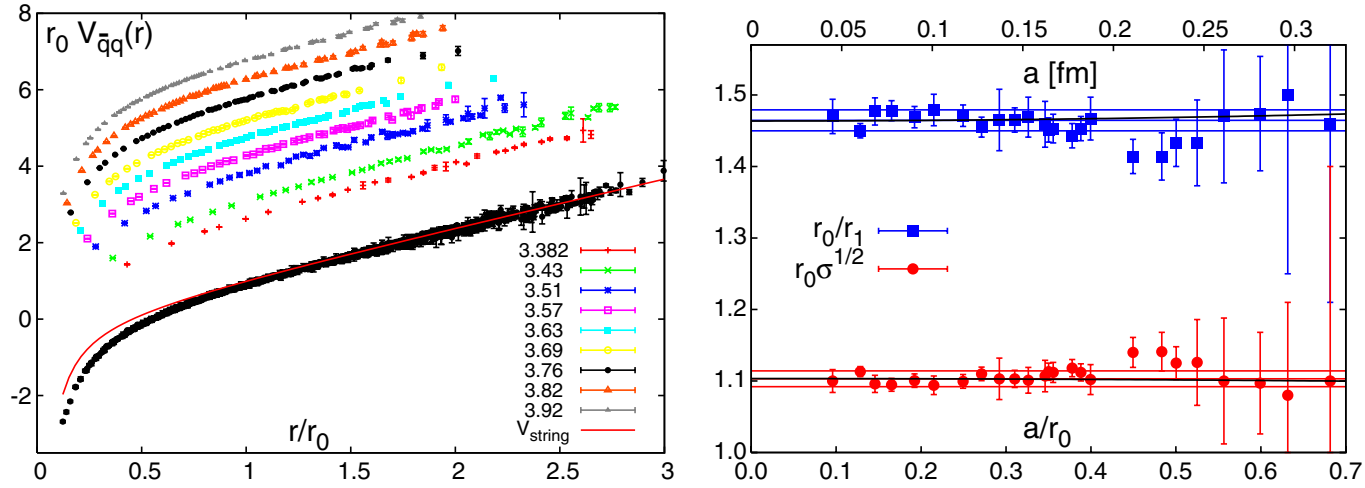

FIG. 1 (color online). The static quark potential in units of the scale r_0 versus distance r/r_0 (left) and dimensionless combinations of the potential shape parameters r_0/r_1 and $r_0\sqrt{\sigma}$ extracted from fits to these potentials (right). The left-hand figure shows potentials for several values of β taken from our entire simulation interval, $\beta \in [3.15{:}4.08]$. The lowest curve in this figure combines all potentials by matching them to the string potential (solid line) as explained in the text. Curves in the right-hand figure show quadratic fits and a fit to a constant with a 1% error band. The lattice spacing has been converted to physical units using $r_0 = 0.469$ fm.

We note that the result obtained here for r_0/r_1 is in good agreement with the corresponding continuum extrapolated value, $r_0/r_1 = 1.474(7)(18)$, determined with the asqtad action from an analysis of the quark mass dependence of this ratio at two different values of the lattice spacing, $a \simeq 0.12$ fm and $a \simeq 0.09$ fm, respectively [29]. We show results for r_0/r_1 and $r_0\sqrt{\sigma}$ calculated at parameter sets close to the LCP in Fig. 1 (right).

Despite the good scaling behavior of dimensionless combinations of scale parameters deduced from the static potential, one expects, of course, to still find substantial deviations from asymptotic scaling relations that are controlled by universal 2-loop β-functions. For the scale parameter r_0/a we parametrize deviations from asymptotic scaling using a rational function *Ansatz*,

$$\hat{r}_0 \equiv \frac{r_0}{a} = \frac{1 + e_r\hat{a}^2(\beta) + f_r\hat{a}^4(\beta)}{a_r R_2(\beta)(1 + b_r\hat{a}^2(\beta) + c_r\hat{a}^4(\beta) + d_r\hat{a}^6(\beta))}, \tag{22}$$

where

$$R_2(\beta) = \exp\left(-\frac{\beta}{12b_0}\right)\left(\frac{6b_0}{\beta}\right)^{-b_1/(2b_0^2)} \tag{23}$$

denotes the 2-loop β-function of QCD for three massless quark flavors and $\hat{a}(\beta) = R_2(\beta)/R_2(3.4)$. With this parametrization it is straightforward to calculate the β-function R_β entering all basic thermodynamic observables,

$$R_\beta(\beta) = \frac{r_0}{a}\left(\frac{\mathrm{d}r_0/a}{\mathrm{d}\beta}\right)^{-1}. \tag{24}$$

Furthermore, we need a parametrization of the β-dependence of the bare quark masses to determine the second β-function entering the thermodynamic relations, i.e. $R_m(\beta)$ defined in Eq. (14). For this purpose we use a parametrization of the product of the bare light quark mass, $\hat{m}_l$ and $\hat{r}_0$ that takes into account the anomalous scaling dimension of quark masses [24],

$$\hat{m}_l\hat{r}_0 = a_m\left(\frac{12b_0}{\beta}\right)^{4/9}P(\beta), \tag{25}$$

with a_m being related to the renormalization group invariant quark mass in units of r_0 and $P(\beta)$ being a sixth order rational function that parametrizes deviations from the leading order scaling relation for the bare quark mass,

$$P(\beta) = \frac{1 + b_m\hat{a}^2(\beta) + c_m\hat{a}^4(\beta) + d_m\hat{a}^6(\beta)}{1 + e_m\hat{a}^2(\beta) + f_m\hat{a}^4(\beta) + g_m\hat{a}^6(\beta)}. \tag{26}$$

This *Ansatz* insures that the parametrization for the two β-functions as well as the parametrization of their product, $R_\beta(\beta)R_m(\beta)$, reproduces the universal 2-loop results given in Eqs. (9) and (19).

In Fig. 2 we show our results for $\hat{r}_0 = r_0/a$ and $\hat{m}_l\hat{r}_0$ together with the fits described above. The fit parameters defining the quark masses on the LCP have been obtained from χ^2-fits in the interval $\beta \in [3.1, 4.08]$. Results for the fit parameters are given in Table II. In addition we find $a_m = 0.0190(9)$ which turns into a value of 8.0(4) MeV in physical units. Fit results for r_0/a differ from the actually calculated values given in Table II by less than 1%.

Like in the pure gauge theory calculations of the equation of state, we also find for QCD with light dynamical quarks that, in the parameter range of interest for finite temperature calculations, β-functions deviate significantly from the asymptotic scaling form. In particular, we find a dip in R_β at $\beta \simeq 3.43$. For small values of N_τ, the interest-

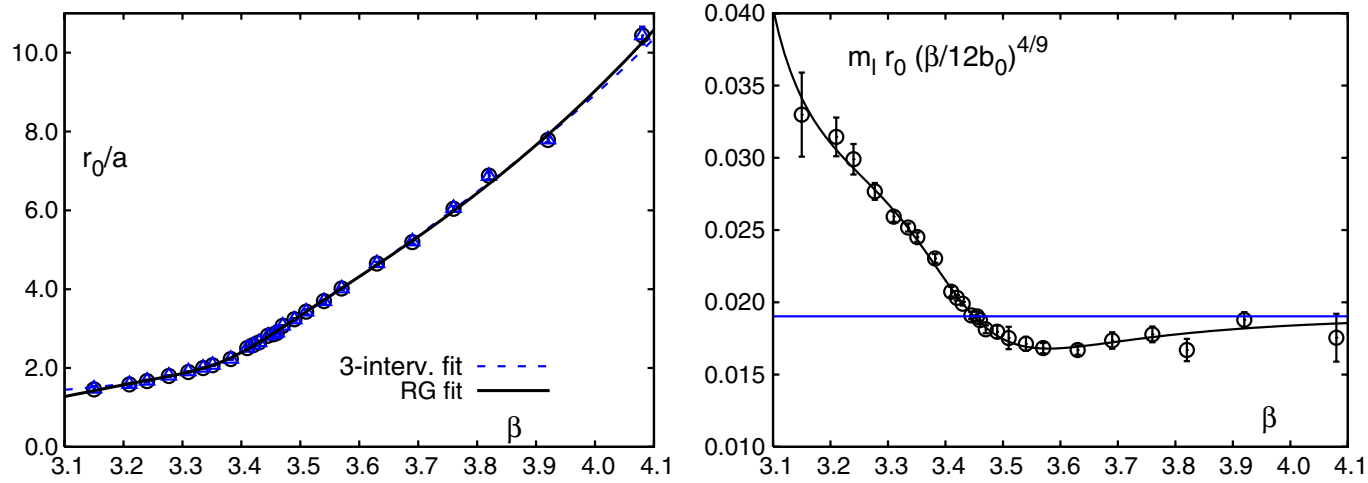

FIG. 2 (color online). The scale parameter $\hat{r}_0 \equiv r_0/a$ versus $\beta = 6/g^2$ (left) and its product with the bare light quark mass on the LCP (right). The two curves shown in the left-hand part of this figure correspond to two different fit *Ansätze*. As explained in the text in addition to the renormalization group motivated *Ansatz* given in Eq. (22) the result from a 3-interval fit is shown. The curve in the right-hand part of the figure shows a fit based on the *Ansatz* given in Eqs. (25) and (26).

TABLE II. Parameters of the fit of the scale parameter r_0 in lattice units based on the *Ansatz* given in Eq. (22) (lower half) and the fit of the renormalization group invariant combination of light quark masses and r_0 [Eq. (25)] on the line of constant physics (upper half). The χ_2/d.o.f for these fits are 1.5 for 19 degrees of freedom (lower half) and 0.84 for 18 degrees of freedom (upper half).

b_m	c_m	d_m	e_m	f_m	g_m
−2.149(121)	1.676(178)	−0.365(144)	−2.290(162)	1.829(425)	−0.356(335)
a_r	b_r	c_r	d_r	e_r	f_r
13.250(363)	−1.201(91)	0.054(196)	0.406(109)	−1.682(103)	0.823(76)

ing parameter range thus includes the crossover region from the strong to weak coupling regime.

We use the interpolating fits for $\hat{r}_0$ and $\hat{m}_l\hat{r}_0$ to determine the two β-functions R_β and R_m that enter the calculations of thermodynamic quantities. As all basic thermodynamic observables are directly proportional to R_β, we should check the sensitivity of R_β on the particular interpolation form used. We thus have used a completely different interpolation that restricts the renormalization group motivated *Ansatz* to the small coupling regime, $\beta \geq 3.52$, and uses purely rational functions to piecewise fit 2 intervals at smaller β. We find that results for R_β are sensitive to the fit *Ansatz* only for small β-values, i.e. $\beta \lesssim 3.25$, where the dependence of $\hat{r}_0$ on β becomes weak. As discussed later the uncertainty on R_β at small values of the coupling only affects the three smallest temperatures used for the analysis of the equation of state on the $N_\tau = 4$ lattices.

Using the parametrizations of $\hat{r}_0$ and $\hat{m}_l\hat{r}_0$ given in Eq. (22) and (25) as well as the above discussed piecewise interpolation of $\hat{r}_0$ we now can derive the two β-functions $R_\beta(\beta)$ and $R_m(\beta)$. In Fig. 3 we show R_β as well as the combination $-R_\beta R_m$ which enters the calculation of the gluonic and fermionic contributions to $(\epsilon - 3p)/T^4$. For $\hat{r}_0$ as well as for the two β-functions, we show results obtained with our two different fit *Ansätze*. As can be seen, the different fit forms lead to differences in the fit result at the edges of the parameter range analyzed. We take care of this in our analysis of the equation of state by averaging over the results obtained with the two different fit *Ansätze* and by including the difference of both fit results as a systematic error. We note that the β-function R_β has a minimum at $\beta \simeq 3.43$. This characterizes the transition from strong to weak coupling regions and is similar to what is known from β-functions determined in pure gauge theory [9] as well as in QCD with heavier quark masses [10]. The details of this region will differ in different discretization schemes as the QCD β-functions are universal only up to 2-loop order in perturbation theory. In order to understand the origin of cutoff effects in thermodynamic observables it is, however, important to have good control over R_β in this nonuniversal regime as well, as R_β enters the calculation of all relevant lattice observables as an overall multiplicative factor.[3]

[3]We note that in order to insure thermodynamic consistency the β-function used in the definition of thermodynamic quantities has to be determined from the cutoff dependence of the observable used to set the temperature scale, i.e. r_0/a in our study.

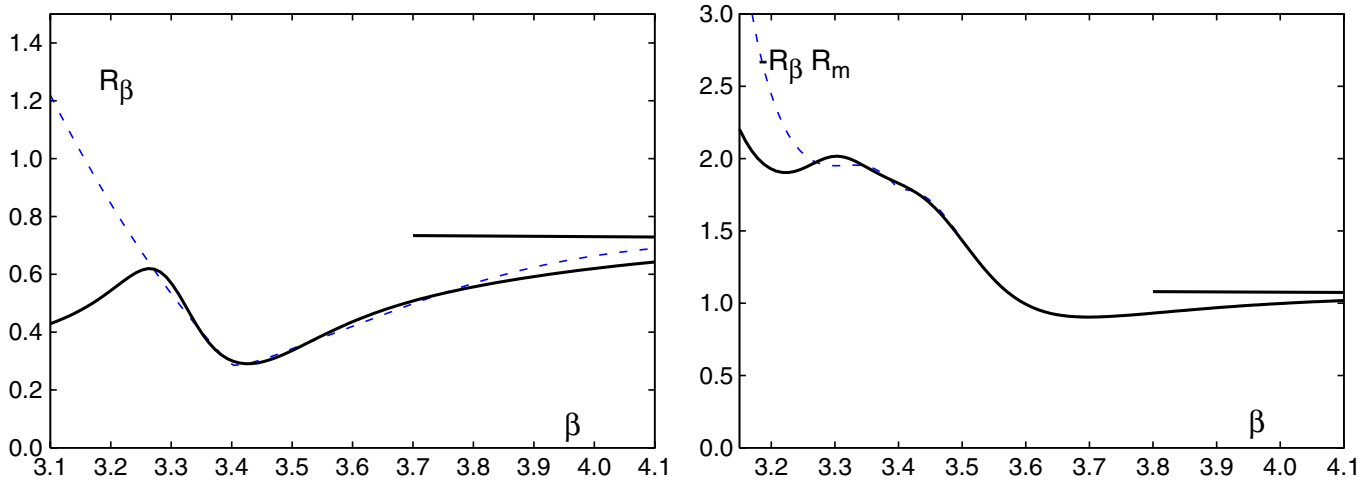

FIG. 3 (color online). The β-function on the LCP [Eq. (24)] (left) and the product $R_\beta R_m$ (right). The horizontal lines show the weak coupling behavior given in Eqs. (9) and (19). The two curves result from two different fits of $\hat{r}_0$ as discussed in the text.

V. BULK THERMODYNAMICS

A. The trace anomaly: $(\epsilon - 3p)/T^4$

The basic lattice observables needed to determine the QCD equation of state with our tree-level improved gauge and fermion actions are expectation values of the gauge action as well as the light and strange quark chiral condensates calculated on the LCP on finite ($N_\tau \ll N_\sigma$) and zero ($N_\tau \gtrsim N_\sigma$) temperature lattices. We have performed finite temperature calculations on lattices with temporal extent $N_\tau = 4$, 6 and 8. In all cases the spatial extent of the lattices (N_σ) was at least 4 times larger than the temporal extent (N_τ), i.e. most finite temperature calculations have been performed on lattices of size $16^3 4$ and $24^3 6$, respectively. In particular at high temperature, we found it important to increase the spatial volume in our calculations on $N_\tau = 6$ lattices to check for possible finite volume effects and also to add a few calculations on $N_\tau = 8$ lattices to get control over the cutoff dependence seen in the trace anomaly. In these cases, calculations on $32^3 6$ and $32^3 8$ lattices have been performed. For all parameter sets, corresponding zero temperature calculations have been performed on lattices of size $16^3 32$ and $24^3 32$. In a few cases we used lattices of size $24^2 \cdot 32 \cdot 48$ as well as 32^4. The length of individual calculations on the finite temperature lattices varied between 6500 and 35 000 trajectories on the $N_\tau = 4$ lattices and 5000 to 17 600 iterations on the $N_\tau = 6$ lattices, where Metropolis updates were done after hybrid Monte Carlo evolutions of trajectory length $\tau_{MD} = 0.5$. At all values of the gauge couplings the length of runs on zero temperature lattices has been adjusted such that the statistical errors of basic observables, e.g. action expectation values, are of similar magnitude as in the $T > 0$ runs. This typically required 2500 to 6000 trajectories. With this amount of statistics, we achieved statistical errors on the basic thermodynamic observable, $(\epsilon - 3p)/T^4$, of below 20% at all temperatures. In fact, they are below 10% in the temperature interval $T \in [180\ \text{MeV}, 700\ \text{MeV}]$ and are less than 5% for $T \in [195\ \text{MeV}, 300\ \text{MeV}]$.

The basic zero and finite temperature observables needed to calculate the trace anomaly in units of the fourth power of the temperature, $\Theta^{\mu\mu}(T)/T^4 = (\epsilon - 3p)/T^4$, from Eq. (7) are summarized in Tables III, IV, V, and VI. To extract $\Theta^{\mu\mu}(T)/T^4$ one furthermore needs to know the derivatives of bare couplings and quark masses, R_β and R_m. Their calculation from zero temperature observables has been discussed in the previous section. With this input, we obtain the result for $\Theta^{\mu\mu}(T)/T^4$, shown in Fig. 4 for the entire range of temperatures explored by us. Here, and in all subsequent figures, the temperature scale has been determined from our results for r_0/a, which characterizes the slope of the static quark potential and has been extracted from the zero temperature potential as discussed in the previous section. On lattices with temporal extent N_τ we then have $Tr_0 \equiv \hat{r}_0/N_\tau$. Whenever we show in the following temperatures in units of MeV we use $r_0 = 0.469$ fm [26] to convert Tr_0 to a MeV-scale. We will, however, show in all figures both scales which should allow us to compare the results presented here unambiguously with any other lattice calculation performed within a different regularization scheme.

In QCD with light (u, d)-quarks and a heavier strange quark the trace anomaly receives, in addition to the gluonic contribution to the trace over the energy-momentum tensor, also contributions from the light and heavy quark chiral condensates [Eqs. (16) and (17)]. In the chiral limit only the former contributes and all fermionic contributions enter indirectly through modifications of the gauge field background. It thus is interesting to check the relative importance of direct contributions from the chiral condensates to $(\epsilon - 3p)/T^4$. In Fig. 5 we show the fermion contribution $\Theta_F^{\mu\mu}/T^4$ to the total trace anomaly shown in Fig. 4. The right-hand part of this figure shows the relative magnitude of the light and strange quark contributions. As

TABLE III. Expectation values of the pure gauge action density, light and strange quark chiral condensates calculated on zero temperature lattices of size $N_\sigma^3 N_\tau$. Also given is the number of trajectories generated at each value of the gauge coupling β with light quarks of mass $\hat{m}_l$ and bare strange quark mass $\hat{m}_s = 10\hat{m}_l$.

β	$100\hat{m}_l$	$N_\sigma^3 \cdot N_\tau$	#traj.	$\langle s_G \rangle_0$	$\langle \bar{\psi}\psi \rangle_{l,0}$	$\langle \bar{\psi}\psi \rangle_{s,0}$
3.150	1.100	$16^3 \cdot 32$	4544	4.825 64(21)	0.287 27(11)	0.392 677(53)
3.210	1.000	$16^3 \cdot 32$	5333	4.689 44(27)	0.252 84(14)	0.358 813(80)
3.240	0.900	$16^3 \cdot 32$	5110	4.614 41(29)	0.231 56(16)	0.333 957(88)
3.277	0.765	$16^3 \cdot 32$	3408	4.516 60(41)	0.202 32(17)	0.298 34(12)
3.290	0.650	$16^3 \cdot 32$	3067	4.476 96(37)	0.188 07(19)	0.275 06(14)
3.335	0.620	$16^3 \cdot 32$	3689	4.360 44(25)	0.154 29(17)	0.244 25(10)
3.351	0.591	$16^3 \cdot 32$	7005	4.318 80(34)	0.141 75(20)	0.230 45(13)
3.382	0.520	$16^3 \cdot 32$	5051	4.234 99(26)	0.115 15(14)	0.199 22(11)
3.410	0.412	$16^3 \cdot 32$	5824	4.159 90(43)	0.090 13(27)	0.162 56(20)
3.420	0.390	$24^3 \cdot 32$	2448	4.136 16(20)	0.083 03(17)	0.153 04(12)
3.430	0.370	$24^3 \cdot 32$	1849	4.112 17(29)	0.076 06(15)	0.143 64(11)
3.445	0.344	$24^3 \cdot 32$	1707	4.077 70(23)	0.066 50(10)	0.130 718(86)
3.455	0.329	$24^3 \cdot 32$	2453	4.056 05(36)	0.060 98(24)	0.123 14(18)
3.460	0.313	$16^3 \cdot 32$	2513	4.044 71(35)	0.057 33(25)	0.117 34(17)
3.470	0.295	$24^3 \cdot 32$	3079	4.023 46(18)	0.052 37(10)	0.109 388(88)
3.490	0.290	$16^3 \cdot 32$	4300	3.984 56(31)	0.044 24(22)	0.100 72(15)
3.510	0.259	$16^3 \cdot 32$	2279	3.946 49(29)	0.036 57(21)	0.087 64(14)
3.540	0.240	$16^3 \cdot 32$	4067	3.893 02(37)	0.028 16(22)	0.075 13(17)
3.570	0.212	$24^3 \cdot 32$	2400	3.843 92(17)	0.021 767(89)	0.062 829(68)
3.630	0.170	$24^3 \cdot 32$	3232	3.752 91(10)	0.013 176(93)	0.045 175(67)
3.690	0.150	$24^3 \cdot 32$	2284	3.669 908(81)	0.008 740(85)	0.035 734(47)
3.760	0.130	$24^2 \cdot 32 \cdot 48$	2538	3.580 005(77)	0.005 781(55)	0.027 805(20)
3.820	0.125	$32^3 \cdot 32$	2913	3.508 124(74)	0.004 467(68)	0.024 666(37)
3.920	0.110	$32^3 \cdot 32$	4677	3.396 477(51)	0.002 967(69)	0.019 635(15)
4.080	0.081	$32^3 \cdot 32$	5607	3.234 961(31)	0.001 546(43)	0.012 779(16)

TABLE IV. Expectation values of the pure gauge action density, light and strange quark chiral condensates calculated on lattices with temporal extent $N_\tau = 4$. The last two columns give the trace anomaly, $\epsilon - 3p$, and the pressure, p, in units of T^4.

β	$100\hat{m}_l$	N_σ^3	#traj.	$\langle s_G \rangle_\tau$	$\langle \bar{\psi}\psi \rangle_{l,\tau}$	$\langle \bar{\psi}\psi \rangle_{s,\tau}$	$(\epsilon - 3p)/T^4$	p/T^4
3.150	1.100	16^3	16 016	4.824 13(46)	0.281 65(22)	0.390 82(12)	0.54(29)	0.0639
3.210	1.000	16^3	21 170	4.685 25(41)	0.243 57(19)	0.355 22(12)	1.03(27)	0.1492
3.240	0.900	16^3	18 741	4.609 04(46)	0.219 62(26)	0.329 20(16)	1.23(18)	0.2060
3.277	0.765	16^3	12 893	4.5001(12)	0.177 84(83)	0.286 88(47)	3.18(25)	0.3208
3.290	0.650	16^3	30 169	4.451 42(58)	0.151 32(49)	0.256 54(28)	4.61(25)	0.4037
3.335	0.620	16^3	17 327	4.285 41(91)	0.049 64(84)	0.190 82(51)	10.77(20)	1.0757
3.351	0.591	16^3	12 427	4.2453(11)	0.037 44(76)	0.174 23(59)	9.68(18)	1.4748
3.382	0.520	16^3	8111	4.166 23(92)	0.018 75(19)	0.137 97(43)	7.70(12)	2.2418
3.410	0.412	16^3	16 000	4.104 65(41)	0.011 657(41)	0.102 29(15)	5.56(12)	2.8435
3.460	0.313	16^3	10 208	4.009 31(64)	0.007 148(28)	0.068 78(17)	3.57(11)	3.5917
3.490	0.290	16^3	9422	3.959 41(38)	0.006 156 3(83)	0.060 172(57)	2.668(71)	3.8864
3.510	0.259	16^3	10 000	3.925 64(36)	0.005 256 8(56)	0.051 830(48)	2.249(56)	4.0322
3.540	0.240	16^3	6258	3.878 12(62)	0.004 627 0(88)	0.045 837(76)	1.687(76)	4.1947
3.570	0.212	16^3	21 196	3.832 12(28)	0.003 904 4(27)	0.038 807(22)	1.378(51)	4.3116
3.630	0.170	16^3	10 000	3.745 81(27)	0.002 912 2(17)	0.029 047(16)	0.896(49)	4.4751
3.690	0.150	16^3	7117	3.665 59(24)	0.002 431 2(11)	0.024 276(10)	0.592(38)	4.5789
3.760	0.130	16^3	33 378	3.577 27(13)	0.001 998 46(36)	0.019 966 2(36)	0.404(22)	4.6498
3.820[a]	0.110	16^3	32 011	3.506 20(13)	0.001 627 76(26)	0.016 268 3(26)	0.273(28)	4.6830
3.920	0.110	32^3	6530	3.395 380(89)	0.001 544 11(10)	0.015 433 7(10)	0.188(21)	4.7156

[a]Note that at $\beta = 3.82$ simulations on $N_\tau = 4$ and 6 lattices have been performed at slightly different quark masses.

TABLE V. Expectation values of the pure gauge action density, light and strange quark chiral condensates calculated on lattices with temporal extent $N_\tau = 6$. The last two columns give the trace anomaly, $\epsilon - 3p$, and the pressure, p, in units of T^4.

β	$100\hat{m}_l$	N_σ^3	#traj.	$\langle s_G \rangle_\tau$	$\langle \bar{\psi}\psi \rangle_{l,\tau}$	$\langle \bar{\psi}\psi \rangle_{s,\tau}$	$(\epsilon - 3p)/T^4$	p/T^4
3.335	0.620	24^3	14 090	4.359 80(34)	0.152 42(19)	0.243 67(13)	0.51(25)	0.0480
3.351	0.591	24^3	17 610	4.317 01(34)	0.138 65(20)	0.229 23(14)	1.19(25)	0.0686
3.382	0.520	24^3	15 530	4.233 36(35)	0.111 03(20)	0.197 73(14)	0.97(19)	0.1393
3.410	0.412	24^3	10 350	4.157 10(36)	0.082 51(31)	0.159 47(19)	1.58(24)	0.2606
3.420	0.390	24^3	9550	4.130 75(41)	0.072 14(39)	0.148 12(24)	2.68(19)	0.3347
3.430	0.370	24^3	11 520	4.104 98(50)	0.061 10(54)	0.136 71(31)	3.57(23)	0.4400
3.445	0.344	24^3	14 380	4.066 34(49)	0.042 31(68)	0.119 37(35)	5.64(28)	0.6766
3.455	0.329	24^3	9050	4.041 26(43)	0.029 28(64)	0.107 88(36)	7.39(32)	0.8982
3.460	0.313	24^3	7690	4.029 13(42)	0.023 74(46)	0.100 61(31)	7.82(34)	1.0240
3.470	0.295	24^3	9190	4.008 34(33)	0.017 15(29)	0.091 12(24)	7.73(26)	1.2885
3.490	0.290	24^3	8360	3.970 23(30)	0.011 87(19)	0.081 85(26)	7.58(27)	1.7784
3.510	0.259	24^3	7880	3.933 93(23)	0.008 204(59)	0.068 22(14)	6.80(20)	2.2005
3.540	0.240	24^3	6920	3.883 47(21)	0.006 247(31)	0.057 47(15)	5.48(23)	2.7123
3.570	0.212	24^3	7310	3.836 71(17)	0.004 923(12)	0.047 364(56)	4.31(19)	3.0925
3.630	0.170	24^3	4760	3.748 30(17)	0.003 426 3(61)	0.033 892(45)	2.98(17)	3.6137
3.690	0.150	24^3	5190	3.666 97(15)	0.002 765 6(24)	0.027 530(19)	2.09(14)	3.9362
3.760	0.130	24^3	8860	3.578 01(12)	0.002 225 1(10)	0.022 203 1(93)	1.49(10)	4.1681
3.820	0.125	32^3	7870	3.506 568(90)	0.002 035 46(42)	0.020 324 7(40)	1.23(11)	4.3136
3.920	0.110	32^3	9322	3.395 328(56)	0.001 676 42(12)	0.016 750 4(12)	0.973(86)	4.5057
4.080	0.081	32^3	6806	3.234 336(54)	0.001 140 13(10)	0.011 397 6(10)	0.599(78)	4.7085

TABLE VI. Expectation values of the pure gauge action density, light and strange quark chiral condensates calculated on lattices with temporal extent $N_\tau = 8$. The last column gives the trace anomaly, $\epsilon - 3p$, in units of T^4.

β	$100\hat{m}_l$	N_σ^3	#traj.	$\langle s_G \rangle_\tau$	$\langle \bar{\psi}\psi \rangle_{l,\tau}$	$\langle \bar{\psi}\psi \rangle_{s,\tau}$	$(\epsilon - 3p)/T^4$
3.820	0.125	32^3	15 100	3.507 493(335)	0.002 144 9(31)	0.021 365 4(187)	2.37(23)
3.920	0.110	32^3	27 100	3.395 797(61)	0.001 743 14(39)	0.017 407 3(31)	1.72(19)
4.080	0.081	32^3	24 100	3.234 705(68)	0.001 175 43(14)	0.011 748 8(14)	0.75(13)

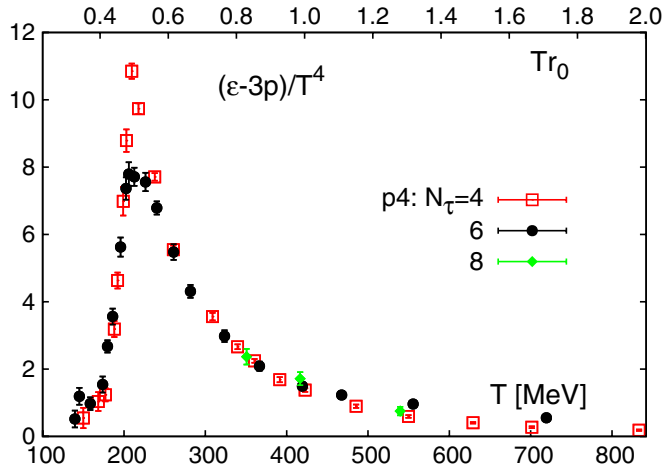

FIG. 4 (color online). The trace anomaly $\Theta^{\mu\mu}(T) \equiv \epsilon - 3p$ in units of T^4 versus temperature obtained from calculations on lattices with temporal extent $N_\tau = 4$, 6 and 8. The temperature scale, Tr_0 (upper x-axis) has been obtained using the parametrization given in Eq. (22), and T [MeV] (lower x-axis), has been extracted from this using $r_0 = 0.469$ fm.

can be seen they are of similar size close to the transition temperature. With increasing temperature, however, the importance of the light quark contribution rapidly drops and becomes similar to the ratio of light to strange quark masses at about twice the transition temperature. As can be seen in Fig. 5 (left) the total fermionic contribution shows a significant cutoff dependence. This partly arises from the large change of the product of β-functions, $R_\beta R_m$ that still deviates a lot from the asymptotic weak coupling value in the range of couplings relevant for the $N_\tau = 4$ and 6 calculations, respectively [see Fig. 3 (right)]. The influence of this cutoff dependence on the calculation of the total trace anomaly, however, is strongly reduced as the contribution of $\Theta_F^{\mu\mu}/T^4$ only amounts to about 20% in the transition region and already drops below 10% at about $1.5T_c$.

As all other thermodynamic observables will eventually be deduced from $(\epsilon - 3p)/T^4$ using standard thermodynamic relations, we should analyze its structure carefully. Bulk thermodynamics of QCD in different temperature intervals addresses quite different physics. This includes

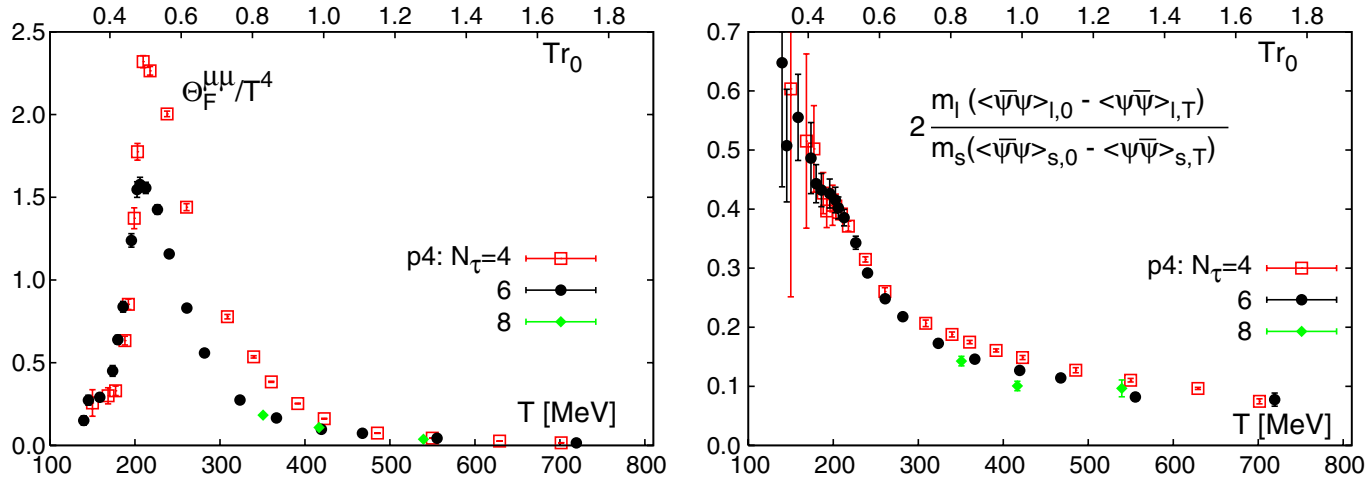

FIG. 5 (color online). The fermionic contribution to the trace anomaly (left) and the ratio of the light and strange quark contributions to $\Theta_F^{\mu\mu}/T^4$ (right).

(i) the low temperature regime, which in the vicinity of the transition temperature often is compared with the physics of a resonance gas and which at lower temperatures is sensitive to properties of the hadron spectrum controlled by chiral symmetry breaking; (ii) the genuine nonperturbative physics in the transition region and at temperatures above but close to the crossover region which is probed experimentally at RHIC and presumably is a still strongly interacting medium with a complicated quasiparticle structure; and (iii) the high temperature regime, which eventually becomes accessible to resummed perturbative calculations. In numerical calculations on a lattice these three regimes also deserve a separate discussion as discretization effects influence lattice calculations in these regimes quite differently. Before proceeding to a calculation of other bulk thermodynamic observables we therefore will discuss in the following three subsections properties of $(\epsilon - 3p)/T^4$ in three temperature intervals: (i) $T \lesssim$ 200 MeV or $T \lesssim T_c$, (ii) 200 MeV $\lesssim T \lesssim$ 300 MeV or $1.0 \lesssim T/T_c \lesssim 1.5$ and (iii) $T \gtrsim$ 300 MeV or $T \gtrsim 1.5T_c$.

1. Trace anomaly at low temperatures

In Fig. 6 we show the low temperature part of $(\epsilon - 3p)/T^4$ obtained from our calculations with the p4fat3 action on lattices with temporal extent $N_\tau = 4$ and 6 and spatial size $N_\sigma/N_\tau = 4$. We compare these results with calculations performed with the asqtad action [11] for $N_\tau = 6$. These latter calculations have been performed on lattices with smaller spatial extent, $N_\sigma/N_\tau = 2$, and results are based on lower statistics. These calculations are, however, consistent with our findings. We also note that results obtained for two different values of the lattice cutoff, $N_\tau = 4$ and 6, are compatible with each other.

In the transition region from high to low temperature it is generally expected that thermodynamic quantities can be described quite well by a hadron resonance gas (HRG) [6]; the freeze-out of hadrons in heavy ion experiments takes place in this region and observed particle abundances are, in fact, well described by a HRG model [30]. Also a comparison of lattice results for the EOS with heavier quarks with a resonance gas model *Ansatz* was quite satisfactory [31] but required the use of a suitably adjusted hadron mass spectrum. As we now can perform lattice calculations with almost physical quark mass values a

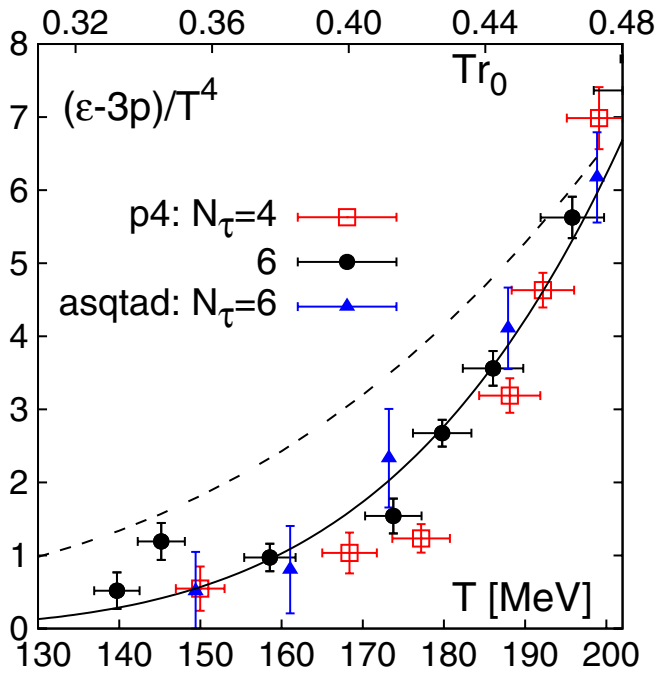

FIG. 6 (color online). Comparison of the low temperature part of $(\epsilon - 3p)/T^4$ calculated on lattices with temporal extent $N_\tau = 4$ and 6 with a resonance gas model that includes all resonances up to mass 2.5 GeV (dashed curve). The solid curve shows a polynomial fit to the $N_\tau = 6$ data obtained with the p4fat3 action. Data for calculations with the asqtad action are taken from [11].

more direct comparison using the HRG model with physical quark mass values should be appropriate.

We use a HRG model constructed from all resonances, with masses taken from the particle data book up to a maximal value $m_{\rm max} = 2.5$ GeV,

$$\left(\frac{\epsilon - 3p}{T^4}\right)_{\rm low-T} = \sum_{m_i \le m_{\rm max}} \frac{d_i}{2\pi^2} \sum_{k=1}^{\infty} (-\eta_i)^{k+1} \frac{1}{k} \times \left(\frac{m_i}{T}\right)^3 K_1(k m_i/T). \quad (27)$$

Here different particle species of mass m_i have degeneracy factors d_i and $\eta_i = -1(+1)$ for bosons (fermions). A comparison of the HRG model with the lattice results is shown as the upper curve in Fig. 6.

As can be seen in this figure the HRG model captures the qualitative features of the lattice results on $(\epsilon - 3p)/T^4$ quite well, although the lattice data seem to drop somewhat faster at low temperature. Whether this points towards a failure of the HRG model at lower temperatures, or is due to difficulties in correctly resolving the low energy hadron spectrum in the current calculations on still rather coarse lattices, will require more detailed studies on finer ($N_\tau = 8$) lattices in the future. We will return to this question in Sec. VII.

We also note that the current lattice calculations are performed with light quark masses that are a factor two larger than the physical ones. Reducing the light quark masses to their physical values will shift the lattice data to smaller temperatures and will thus improve the comparison with the HRG model. From the known systematics of the quark mass dependence of other thermodynamic quantities, e.g. the transition temperature, chiral condensates or Polyakov loop expectation values [18], one can estimate this shift to be less than 5 MeV. Moreover, we note that the scale r_0 used to convert lattice results to physical units has an error of about 2%. This is indicated in Fig. 6 by a horizontal error bar for the data. Within this error all data may be shifted coherently.

The low temperature region of the QCD EOS clearly deserves more detailed study in the future.

2. Trace anomaly in the strongly nonperturbative regime

At temperatures just above the transition temperature, $(\epsilon - 3p)/T^4$ shows the largest deviations from the conformal limit, $\epsilon = 3p$. The peak in $(\epsilon - 3p)/T^4$ at a temperature $T_{\rm max}$ that is only slightly larger than the transition temperature T_c constitutes a prominent structure of the trace anomaly which is relatively easy to determine in a lattice calculation. It is closely related to the softest point in the QCD equation of state [32], i.e. the minimum of p/ϵ as function of the energy density. $T_{\rm max}$ thus plays an important role for the construction of model equations of state that are consistent with lattice calculations and may be used in hydrodynamic models for the expansion of dense matter created in heavy ion collisions. As $T_{\rm max}$ and, in particular $(\epsilon - 3p)/T^4_{\rm max}$ are easily determined they may also serve as consistency checks between different lattice calculations.

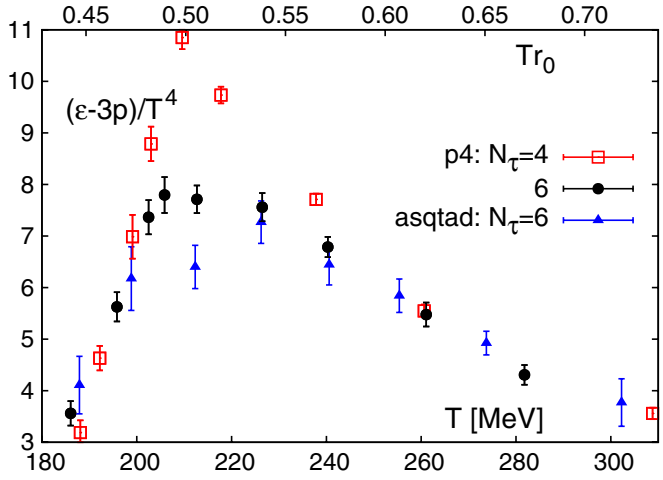

FIG. 7 (color online). The trace anomaly in the vicinity of the transition temperature calculated on lattices with temporal extent $N_\tau = 4$ and 6 on lattices with aspect ratio $N_\sigma/N_\tau = 4$. Data for calculations with the asqtad action are taken from [11] which have been performed on finite temperature lattices with a smaller physical volume corresponding to an aspect ratio $N_\sigma/N_\tau = 2$.

In Fig. 7 we show results for $(\epsilon - 3p)/T^4$ in the intermediate temperature interval 180 MeV $< T <$ 300 MeV. Also shown here are results from calculations performed with the asqtad action on lattice with temporal extent $N_\tau = 6$ [11]. As can be seen these calculations are in quite good agreement with the results obtained with the p4fat3 action on lattice with the same temporal extent but larger spatial volume. Estimates for $T_{\rm max}$ and the peak height on lattices with temporal extent $N_\tau = 4$ and 6 are given in Table VII. Also given there are estimates for the transition temperature $T_c r_0$ obtained previously in a dedicated analysis of the transition temperature on $N_\tau = 4$ and 6 lattices [18]. The values quoted in the table give the fit results obtained from a joint fit of transition temperatures on both lattice sizes for different quark mass values evaluated at the pseudoscalar

TABLE VII. Position of the peak in $(\epsilon - 3p)/T^4$ and its value calculated on lattices with different values of the temporal extent N_τ on a line of constant physics that corresponds to a pion mass of about 220 MeV. Errors on the peak positions have been estimated from cubic fits in the peak region by varying the fit intervals. The second and third columns show the transition temperature determined on the LCP used for this study of the EOS. For $N_\tau = 4$ this had been determined in [18] and for $N_\tau = 6$ in this analysis (see discussion in Sec. VI).

N_τ	$T_c r_0$	T_c [MeV]	$(Tr_0)_{\rm max}$	$T_{\rm max}$ [MeV]	$(\epsilon - 3p)/T^4_{\rm max}$
4	0.484(4)	204(2)	0.50(1)	211(4)	10.8(3)
6	0.466(6)	196(3)	0.49(1)	208(4)	7.8(4)

mass values corresponding to our LCP. We note that the temperature $T_{\rm max}$ is only about 3% larger than the transition temperatures determined from peaks in the chiral susceptibility.

On the coarse $N_\tau = 4$ lattices the analysis of $(\epsilon - 3p)/T^4$ in the transition region is still quite sensitive to the nonperturbative structure of the β-functions, R_β and $R_\beta R_m$ shown in Fig. 3; this region is still close to the strong coupling regime below and in the vicinity of the dip in R_β shown in Fig. 3 (left). This seems to be the main reason for the large differences seen in the peak height for $(\epsilon - 3p)/T^4$ between the $N_\tau = 4$ and 6 lattices. In the latter case the transition and peak region is already in the regime where the lattice β-functions smoothly approach the continuum results. We thus expect that these results are much less affected by this source of lattice artifacts. Nonetheless, a better control over the cutoff dependence in this region clearly is needed and does require calculations on a larger lattice in order to control the continuum extrapolations of $T_{\rm max} r_0$ as well as $(\epsilon - 3p)/T^4_{\rm max}$.

3. Trace anomaly at high temperatures

In Fig. 8 we show results for $(\epsilon - 3p)/T^4$ in the high temperature regime, $T \gtrsim 1.5T_c$. A comparison with data obtained with the asqtad action on lattices with temporal extent $N_\tau = 6$ shows that the results obtained here with the p4fat3 action are compatible with the former for $T \lesssim 400$ MeV ($\sim 2T_c$). The current analysis performed with the p4fat3 action, however, has been extended to much larger temperatures, $T \sim 4T_c$, i.e. into the temperature regime accessible to heavy ion experiments at the LHC.

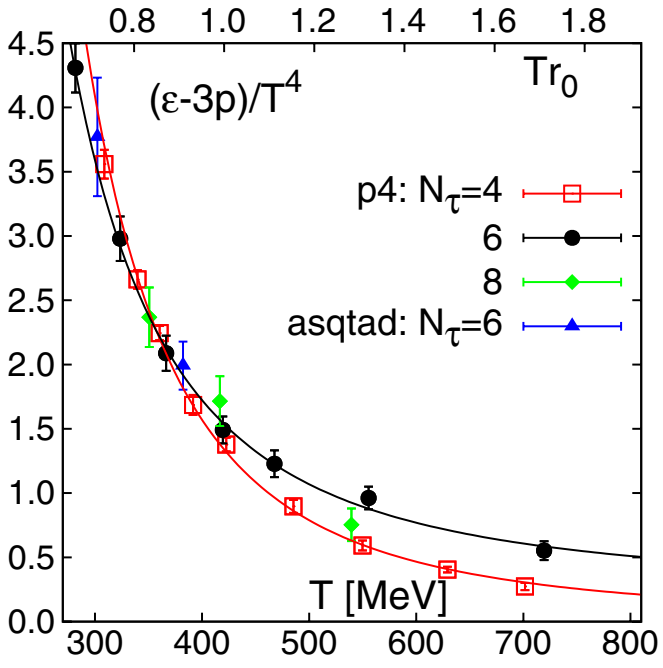

FIG. 8 (color online). The high temperature part of $(\epsilon - 3p)/T^4$ calculated on lattices with temporal extent $N_\tau = 4$, 6 and 8. The curves show fits to the $N_\tau = 4$ and 6 data with the *Ansatz* given in Eq. (29).

For temperatures larger than $T_{\rm max}$ the trace anomaly rapidly drops. Eventually, when the high temperature perturbative regime is reached, the temperature dependence is expected to be controlled by the logarithmic running of the QCD coupling constant. To leading order in high temperature perturbation theory $\Theta^{\mu\mu}(T)$ for massless quarks is given by [1]

$$\frac{\epsilon - 3p}{T^4} = \frac{1}{3} b_0 \left(1 + \frac{5}{12} n_f\right) g^4(T) + O(g^5), \qquad (28)$$

with $n_f = 3$ for massless 3-flavor QCD, which corresponds to the high temperature limit for our (2 + 1)-flavor QCD calculations performed on a LCP with fixed nonzero quark mass values.

For temperatures larger than about $2.0T_c$ results for $\Theta^{\mu\mu}(T)/T^4$ obviously are sensitive to lattice cutoff effects. The results on $N_\tau = 6$ lattices drop significantly slower with temperature than the $N_\tau = 4$ results. In order to make sure that this effect does not superimpose with possible finite volume effects, we increased in this temperature region the spatial lattice size from 24^3 to 32^3. No statistically significant volume effects have been observed for $\Theta^{\mu\mu}(T)/T^4$, although we observe a sensitivity of the zero temperature light and strange quark chiral condensates on the volume; as the condensates contribute less than 10% to the trace anomaly at these high temperature values (see Fig. 5) modifications of the condensates by a few percent contribute insignificantly to finite volume effects in $\Theta^{\mu\mu}(T)/T^4$. Moreover, as the entire fermionic contribution, $\Theta^{\mu\mu}_F(T)/T^4$, to the total trace anomaly is small for $T \gtrsim 400$ MeV, it is obvious that the contribution of the fermion condensates is not the source for the cutoff effects at high temperature. The cutoff dependence seen in Fig. 8 arises from the gluonic sector of $\Theta^{\mu\mu}(T)/T^4$, which of course also receives contributions from virtual quark loops.

In the high temperature region we also added calculations on lattices with temporal extent $N_\tau = 8$ at 3 different values of the temperature. Results from these calculations are summarized in Table VI and are also shown in Fig. 8. As can be seen in this figure results obtained for the trace anomaly on the $N_\tau = 8$ lattice are in good agreement with the $N_\tau = 6$ results suggesting that remaining cutoff effects in this temperature range are small for $N_\tau \geq 6$.

We note that larger values for $\Theta^{\mu\mu}(T)/T^4$ at high temperature also lead to larger values for the pressure, which is obtained from an integral over the trace anomaly, and also results in larger values for the energy and entropy densities, i.e. these quantities approach the Stefan-Boltzmann limit more rapidly on the $N_\tau = 6$ lattices than they did on the $N_\tau = 4$ lattice. It thus is important to get good control over cutoff effects at high temperatures and obtain further confirmation of the results obtained in our $N_\tau = 6$ lattices, and through further calculations, on the $N_\tau = 8$ lattices at higher temperatures.

TABLE VIII. Fit parameters for 2-parameter fits ($N_\tau = 4$) and 3-parameter fits ($N_\tau = 6$) to $(\epsilon - 3p)/T^4$ in the region $T \geq 300$ MeV using the *Ansatz* given in Eq. (29).

N_τ	g^2	b [GeV^2]	c [GeV^4]
4	...	0.101(6)	0.024(1)
6	2.3(7)	0.16(6)	0.013(6)

As discussed previously, $\Theta^{\mu\mu}(T)/T^4$ contains a contribution from the vacuum quark and gluon condensates that gets suppressed by a factor T^4 at high temperature. In the case of a pure gauge theory it has, however, been noted that up to temperatures a few times the transition temperature the dominant powerlike correction to the perturbative high temperature behavior is $\mathcal{O}(T^{-2})$ rather than $\mathcal{O}(T^{-4})$ [33,34]. These qualitative features also show up in our results for $\Theta^{\mu\mu}(T)/T^4$ at temperatures $T \gtrsim 1.5T_c$. In Fig. 8 we show a comparison of the lattice results with such a phenomenologically motivated polynomial fit *Ansatz*,

$$\left(\frac{\epsilon - 3p}{T^4}\right)_{\text{high}-T} = \frac{3}{4} b_0 g^4 + \frac{b}{T^2} + \frac{c}{T^4}. \tag{29}$$

Here we used the parametric form of the leading order perturbative result given in Eq. (28) with a temperature independent coupling g^2 to characterize the high temperature behavior of $(\epsilon - 3p)/T^4$ in the fit interval $T \in [300\ \text{MeV}, 800\ \text{MeV}]$. For $N_\tau = 4$ we only performed a 2-parameter fit as it turned out that the fit does not require the contribution from a constant term ($g^2 \equiv 0$). The fit parameters obtained from fits in the region $T \geq 300$ MeV are given in Table VIII. We note that the vacuum condensate contribution ($\sim c/T^4$) is small compared to the genuine thermal part. The present analysis, however, does not yet allow us to disentangle logarithmic from powerlike (quadratic) corrections.

Of course, it is tempting to relate the coefficient of the quartic term to a bag constant or zero temperature quark and gluon condensate contribution, $c = 4B$. This yields quite a reasonable value, $B^{1/4} = 247(25)$ MeV. Nonetheless, it seems that a more detailed analysis of the scaling behavior in the high temperature region and better control over cutoff effects is needed before a proper running of the gauge coupling can be established that would unambiguously allow one to single out powerlike (quadratic) corrections in the high temperature regime which then would also allow one to establish a connection to the perturbative regime for the trace anomaly.

B. Pressure, energy and entropy density

As indicated in Eq. (4) we obtain the pressure difference,

$$\Delta_p(T) \equiv \frac{p(T)}{T^4} - \frac{p(T_0)}{T_0^4}, \tag{30}$$

by integrating over the trace anomaly weighted with an additional factor of T^{-1} in the interval $[T_0, T]$. We have started our integration at $T_0 = 100$ MeV, or $Tr_0 \simeq 0.24$, by setting the trace anomaly to zero at this temperature. As discussed in the previous section, this leaves us with an uncertainty for the value of the pressure at T_0, which we estimate to be of the order of the pressure in a hadron resonance gas, i.e. $[p(T_0)/T_0^4]_{HG} = 0.265(2)$. The results obtained for $\Delta_p(T)$ from our lattice calculations for the pressure at higher temperatures thus yield p/T^4 up to a systematic uncertainty on $p(T_0)/T_0^4$. We also note again that the normalization at T_0 does not take care of the overall normalization of the pressure at $T = 0$.

To calculate $\Delta_p(T)$ by integrating the numerical results obtained for $\Theta^{\mu\mu}(T)/T^4$ from Eq. (4), we have used straight line interpolations of our results for $\Theta^{\mu\mu}/T^4$ at adjacent values of the temperature. We also used stepwise interpolations obtained by fitting quadratic polynomials to the data in small intervals that are matched to fits in the previous interval. Results of the latter approach are then used to perform the integration in the various regions analytically. Differences between this approach and the straight line interpolations are nowhere larger than 1.5%. We then used the smooth polynomial interpolations to determine the pressure and combined this result with that for $\Theta^{\mu\mu}(T)$ to obtain the energy density. Both are shown in the left-hand part of Fig. 9. The uncertainty arising from the normalization of the pressure at T_0 is indicated as a small vertical bar in the upper right part of this figure. We note that at $T \sim 4T_c$ results for p/T^4 and ϵ/T^4 stay about 10% below the ideal gas value.

In particular, for applications to heavy ion phenomenology and for the use of the QCD equation of state in hydrodynamic modeling of the expansion of matter formed in heavy ion collisions, it is of importance to eliminate the temperature in favor of the energy density and thus obtain the pressure as function of energy density. The ratio p/ϵ is shown in the right-hand part of Fig. 9. As can be seen at low temperature, in the vicinity of the minimum in p/ϵ, results are consistent with values extracted for this quantity from a hadron resonance gas model. We also note that in the high temperature regime it has been found in [35] that the ratio p/ϵ shows little dependence the baryon number density when evaluated on lines of constant entropy per baryon number.

The density dependence of p/ϵ is related to the square of the velocity of sound

$$c_s^2 = \frac{\mathrm{d}p}{\mathrm{d}\epsilon} = \epsilon \frac{\mathrm{d}p/\epsilon}{\mathrm{d}\epsilon} + \frac{p}{\epsilon}. \tag{31}$$

In the high temperature limit as well as in the transition region where the derivative $\mathrm{d}(p/\epsilon)/\mathrm{d}\epsilon$ vanish, c_s^2 is directly given by p/ϵ. We therefore find that the velocity of sound is close to the ideal gas value, $c_s^2 = 1/3$, for energy densities $\epsilon \gtrsim 100$ GeV/fm^3 and drops by a factor of 4 to a

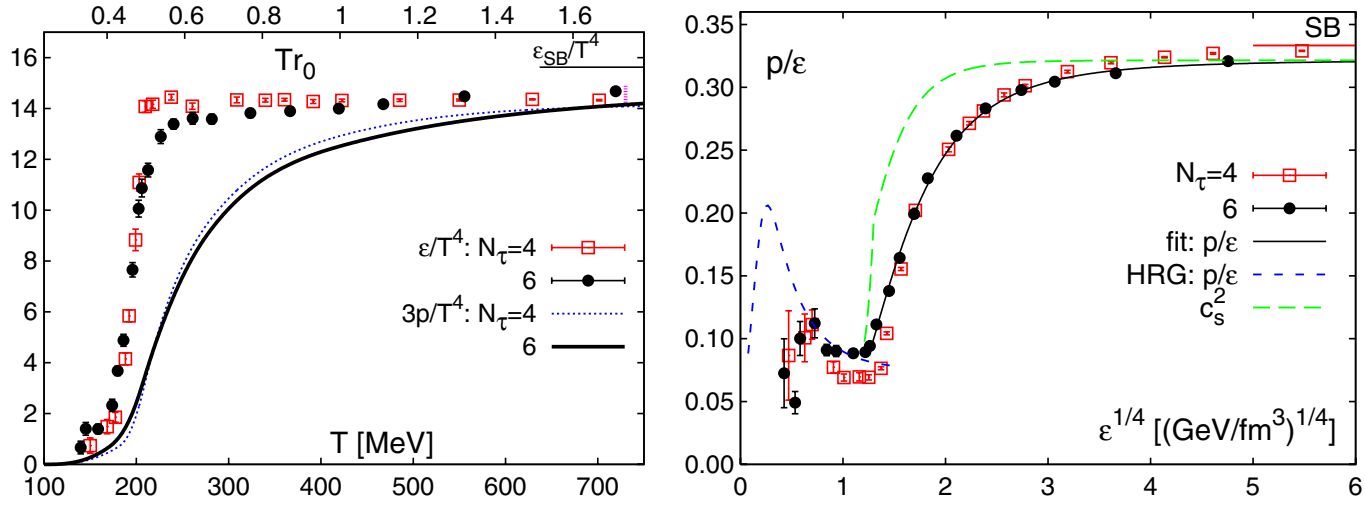

FIG. 9 (color online). Energy density and 3 times the pressure as function of the temperature (left) and the ratio p/ϵ as function of the fourth root of the energy density (right) obtained from calculations on lattices with temporal extent $N_\tau = 4$ and 6. Temperature and energy density scales have been obtained using the parametrization of r_0/a given in Eq. (22) and $r_0 = 0.469$ fm. The small vertical bar in the left-hand figure at high temperatures shows the estimate of the systematic uncertainty on these numbers that arises from the normalization of the pressure at $T_0 = 100$ MeV. The dashed curve (HRG) in the right-hand figure shows the result for p/ϵ in a hadron resonance gas for temperatures $T < 190$ MeV.

minimal value of about $(c_s^2)_{\rm min} \simeq 0.09$ that is reached at $\epsilon \gtrsim$ (1–2) GeV/fm^3. The dependence of p/ϵ on the energy density can be parametrized in the high temperature region with a simple *Ansatz* [35],

$$\frac{p}{\epsilon} = \frac{1}{3}\left(C - \frac{A}{1 + B\epsilon\,\mathrm{fm}^3/\mathrm{GeV}}\right), \tag{32}$$

which then also allows a simple calculation of the velocity of sound, using Eq. (31). We find that the above parametrization yields a good fit of the $N_\tau = 6$ data in the interval $1.3 \leq \epsilon^{1/4}/(\mathrm{GeV/fm}^3)^{1/4} \leq 6$ with a χ^2/dof of 1.3. For the fit parameters we obtain, $C = 0.964(5)$, $A = 1.16(6)$ and $B = 0.26(3)$. This fit and the resulting velocity of sound are also shown in Fig. 9 (right).

At energy densities below $\epsilon \simeq 1$ GeV/fm^3 the lattice calculations indicate a rise of p/ϵ as expected in hadron resonance gas models. However, the current resolution and accuracy of lattice calculations in this regime clearly is not yet sufficient to allow for a detailed comparison between both.

As pointed out in Sec. II the nonperturbative vacuum condensates of QCD show up at high temperature as powerlike corrections to temperature dependence of the trace anomaly and consequently also to pressure and energy density. These vacuum condensate contributions drop out in the entropy density which is shown in Fig. 10. It thus is an observable most suitable for comparisons with (resummed) perturbative calculations [15]. Like energy density and pressure, the entropy also deviates from the ideal gas value by about 10% at $T \sim 4T_c$.

We note that for $T \lesssim 2T_c$ the results obtained with the asqtad action [11] for the entropy density are in good agreement with the results obtained with the p4fat3 action, although at least in the high temperature limit the cutoff dependence of both actions is quite different. This suggests that at least up to temperature $T \simeq 2T_c$ nonperturbative contributions dominate the properties of bulk thermody-

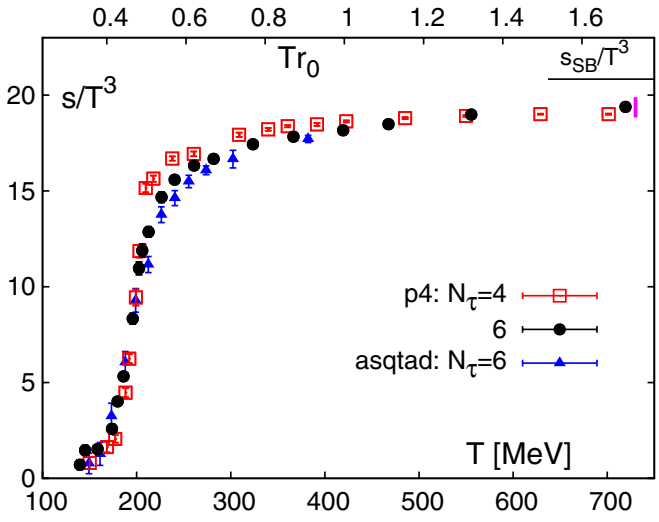

FIG. 10 (color online). Entropy density as function of the temperature obtained from calculations on lattices with temporal extent $N_\tau = 4$ and 6. Temperature and energy density scales have been obtained using the parametrization of r_0/a given in Eq. (22) and $r_0 = 0.469$ fm. The small vertical bar at high temperatures shows the estimate of the systematic uncertainty on these numbers that arises from the normalization of the pressure at $T_0 = 100$ MeV.

namic observables like the entropy density. It also gives rise to the expectation that additional cutoff effects are small. Nonetheless, the result presented in this section on properties of bulk thermodynamic observables clearly need to be confirmed by calculations on lattices with larger temporal extent.

VI. RENORMALIZED POLYAKOV LOOP AND CHIRAL CONDENSATES

As part of our analysis of bulk thermodynamic observables we have gathered a lot of information on the static quark potential at zero temperature. This has been discussed in Sec. IV and results obtained for $V_{\bar{q}q}(r)$ have been used there to determine a temperature scale for our thermodynamic calculations. Furthermore, we have obtained a lot of information on the chiral condensates at zero temperature that entered our calculation of thermodynamic quantities. Together with corresponding results on heavy quark free energies and chiral condensates at finite temperature this allows us to analyze the deconfining properties as well as the change of chiral properties of the finite temperature transition in terms of observables which are related to exact order parameters for deconfinement and chiral symmetry restoration in the infinite quark mass and vanishing quark mass limits of QCD, respectively.

As discussed in the previous sections, the deconfining aspect of the finite temperature transition, i.e. the sudden liberation of partonic degrees of freedom in QCD, is reflected in the rapid change of bulk thermodynamic observables. This is also reflected in the rapid change of the static quark free energy which characterizes the response of a thermal medium to the addition of static quark sources. The static quark free energy, F_q, is related to the Polyakov loop expectation value, $\langle L\rangle \sim \exp(-F_q(T)/T)$,

$$\langle L\rangle = \left\langle \frac{1}{N_\sigma^3}\sum_{\vec{x}} L_{\vec{x}} \right\rangle \quad \text{with} \quad L_{\vec{x}} = \frac{1}{3}\,\mathrm{Tr}\prod_{x_0=1}^{N_\tau} U_{(x_0,\vec{x}),\hat{0}}. \quad (33)$$

It may more rigorously be defined through the asymptotic large distance behavior of static quark-antiquark correlation functions [36],

$$\langle L\rangle^2 = \lim_{|\vec{x}-\vec{y}|\to\infty} \langle L_{\vec{x}} L^\dagger_{\vec{y}}\rangle. \quad (34)$$

The Polyakov loop needs to be renormalized in order to attain a physically meaningful value in the continuum limit. To construct the renormalized Polyakov loop from the bare Polyakov loop expectation values, $\langle L\rangle$, calculated on lattices with temporal extent N_τ at a temperature controlled by the gauge coupling β,

$$L_{\mathrm{ren}}(T) = Z_{\mathrm{ren}}^{N_\tau}(\beta)\langle L\rangle, \quad (35)$$

we can make use of our extensive calculations of the static potential at zero temperature. As outlined in Sec. IV we have extracted renormalization constants, $(c(\beta)a)$, from the matching of the static potential to the string potential. These renormalization constants are given in Table I in terms of the product $c(\beta)r_0$. With this we obtain the renormalization constants for the Polyakov loop as $Z_{\mathrm{ren}}(\beta) = \exp(c(\beta)a/2)$.

Results for the renormalized Polyakov loop are shown in Fig. 11 (left). We note that the cutoff dependence of L_{ren} on lattices with temporal extent $N_\tau = 4$ and 6 is small, which is in agreement with results obtained in studies of L_{ren} in pure $SU(3)$ gauge theories [36]. A similar renormalization of the Polyakov loop obtained in calculations with the 1-link, stout smeared staggered fermion action has been used in [37]. The large cutoff dependence of L_{ren} observed in this case mainly seems to be due to the choice of observable (f_K) that has been used to set the temperature scale. In fact, when using r_0 instead of f_K to determine the lattice

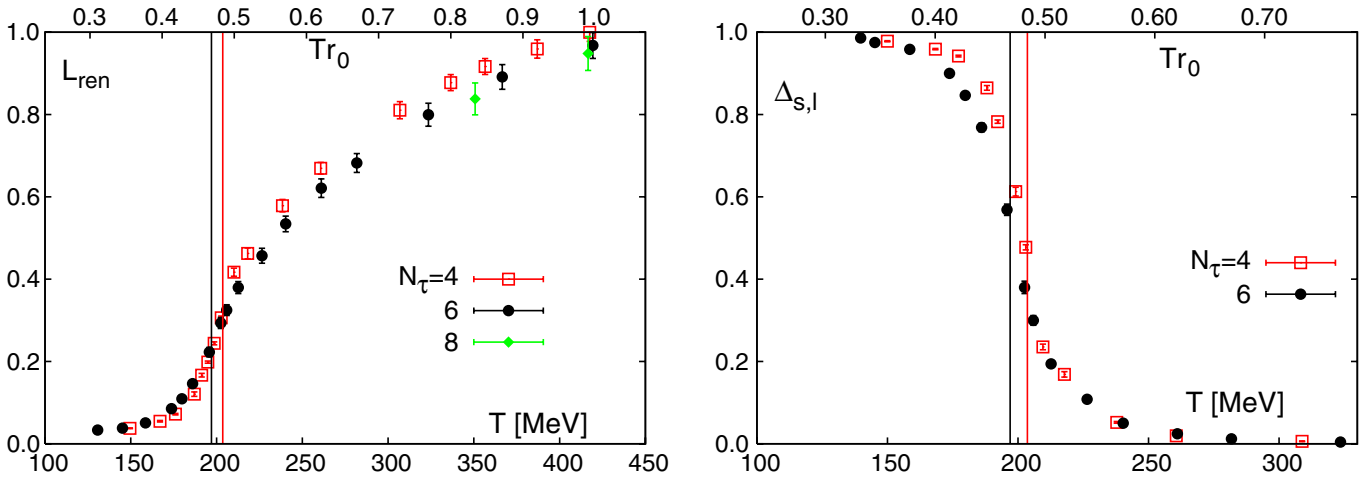

FIG. 11 (color online). Renormalized Polyakov loop on lattices with temporal extent $N_\tau = 4$, 6 and 8 (left) and the normalized difference of light and strange quark chiral condensates defined in Eq. (36). The vertical lines show the location of the transition temperature determined in [18] on lattices with temporal extent $N_\tau = 4$ (right line) and in this analysis for $N_\tau = 6$ (left line).

spacing, and thus the temperature, most of the cutoff dependence of $L_{\rm ren}$ is removed in the data shown in [37].

Another important aspect of the QCD transition is, of course, the change of chiral properties with temperature. This is generally reflected in the temperature dependence of the chiral condensate or related susceptibilities. Also the chiral condensates need to be renormalized to obtain finite, well defined quantities in the continuum limit. To eliminate the quadratic divergences in the linear quark mass dependent correction to the chiral condensates [24] we calculate a suitable combination of light and strange quark condensates at finite temperature. We furthermore normalize this quantity by the corresponding combination of condensates calculated at zero temperature at the same value of the lattice cutoff, i.e. at the same value of the gauge coupling β,

$$\Delta_{l,s}(T) = \frac{\langle\bar{\psi}\psi\rangle_{l,\tau} - \frac{\hat{m}_l}{\hat{m}_s}\langle\bar{\psi}\psi\rangle_{s,\tau}}{\langle\bar{\psi}\psi\rangle_{l,0} - \frac{\hat{m}_l}{\hat{m}_s}\langle\bar{\psi}\psi\rangle_{s,0}}. \tag{36}$$

This eliminates multiplicative renormalization factors.

In Fig. 11 (right) we show results obtained for $\Delta_{l,s}(T)$ on the LCP for $N_\tau = 4$ and 6. In this figure, as well as in the corresponding figure for $L_{\rm ren}(T)$ shown on the left-hand side, we also give estimates for the pseudocritical temperature extracted from the position of the peak in the disconnected part of the light quark chiral susceptibility. For $N_\tau = 4$ this value has been determined previously by us [18] as the quark mass parameters for the LCP used here are close to those used in [18] to determine T_c on the $N_\tau = 4$ lattices for $\hat{m}_l/\hat{m}_s = 0.1$. For $N_\tau = 6$ the choice of the strange quark mass differs slightly from the one used in that earlier study. We therefore performed a new determination of the transition temperature for the $N_\tau = 6$ lattice and the parameters of the LCP used here. From the peak positions of the disconnected parts of the light and strange quark susceptibilities we find $\beta_c(N_\tau = 6) = 3.445(3)$. Using the value for r_0/a quoted for this value of the coupling in Table I we find[4] $T_c r_0 = 0.466(6)$ or $T_c = 196(3)$.

We note that the region of most rapid change in the subtracted and normalized chiral condensate, $\Delta_{l,s}(T)$, is in good agreement with the region where the Polyakov loop expectation value as well as bulk thermodynamic quantities, e.g. the energy and entropy densities, change most rapidly.

VII. DISCUSSION AND CONCLUSIONS

We have presented here a detailed analysis of the QCD equation of state with an almost physical quark mass spectrum. The current calculations have been performed with a physical strange quark mass value and two degenerate light quark masses that are about a factor two larger than the physical average light quark mass value. In a wide temperature range, results have been obtained on large spatial lattices close to the thermodynamic limit for two different values of the lattice cutoff, corresponding to lattices of temporal extent $N_\tau = 4$ and 6. At high temperatures additional calculations on lattices with temporal extent $N_\tau = 8$ have been performed, which allow us to control apparent cutoff effects in this temperature range. All finite temperature calculations have been supplemented with corresponding zero temperature calculations to perform necessary vacuum subtractions and to accurately set the temperature scale.

At high temperature, $T \gtrsim 2T_c$, bulk thermodynamic observables such as pressure, energy and entropy density deviate from the continuum Stefan-Boltzmann values only by about 10% and show little cutoff dependence. This weak cutoff dependence could only be achieved through the use of $\mathcal{O}(a^2)$ improved gauge and fermion actions. On the other hand, a closer look at the trace anomaly, $(\epsilon - 3p)/T^4$, from which these quantities are derived, clearly unravels cutoff effects when comparing results obtained for the $N_\tau = 4$ and 6 lattices; for temperatures $T \gtrsim 2.5T_c$ or equivalently $T \gtrsim 500$ MeV results for $(\epsilon - 3p)/T^4$ on the $N_\tau = 4$ lattices are systematically lower than for $N_\tau = 6$. Additional calculations performed on $N_\tau = 8$ lattices in this high temperature region are consistent with the results obtained on $N_\tau = 6$ lattices and thus suggest that cutoff effects are small on lattice with temporal extent $N_\tau \geq 6$. Of course, this should be confirmed through additional calculations on lattices with temporal extent $N_\tau = 8$ at larger temperatures. On these fine lattices it also will be interesting to analyze in more detail the contribution of charm quarks to the equation of state [38,39].

Getting better control over the temperature dependence of $(\epsilon - 3p)/T^4$ at high temperature clearly is important when one wants to make contact between lattice calculations for, e.g. the entropy density and high temperature perturbation theory. Although our present high statistics analysis seems to have achieved good control over the cutoff dependence of $(\epsilon - 3p)/T^4$ in this high temperature regime, a more extended analysis of the temperature dependence on $N_\tau = 8$ lattices is still needed to make firm contact with perturbative or resummed perturbative calculations.

At low temperatures, $T \lesssim 200$ MeV, the influence of cutoff effects is less apparent. We observe that at a given value of the temperature results for $(\epsilon - 3p)/T^4$ obtained on the $N_\tau = 6$ lattice are systematically larger than those obtained on the $N_\tau = 4$ lattice. This is, in fact, expected and is consistent with the cutoff dependence observed in calculations of the transition temperature on lattices with temporal extent $N_\tau = 4$ and 6 [18]. Also on lattices with temporal extent $N_\tau = 8$ indications for this to happen have

[4]Our earlier analysis for $m_l = 0.1m_s$ on a $16^3 6$ lattice, performed with a 20% larger strange quark mass, gave $T_c r_0 = 0.4768(51)$ or $T_c = 201(2)$.

been found in preliminary studies of chiral and quark number susceptibilities as well as Polyakov loop expectation values [40]. We thus expect that with increasing N_τ, i.e. closer to the continuum limit, the region where $(\epsilon - 3p)/T^4$ and all other thermodynamic observables will start to rise rapidly, continues to shift towards smaller temperatures. A further, although smaller shift of the transition region towards smaller values of the temperature will arise from an extrapolation to physical quark masses. Judging from the known temperature dependence of the transition temperature [18] and other thermodynamic observables, like the Polyakov loop expectation value or quark number susceptibilities [40], this will amount to a shift of the scale by a few MeV. In fact, extrapolations of the transition temperature in quark mass and lattice spacing to the physical point have been performed by several groups for staggered as well as Wilson fermions [18,41,42]. These extrapolations consistently show that the quark mass dependence of the transition temperature is weak. We take the quark mass dependence of the transition temperature as indicator for the shift of the transition region one has to expect in future calculations on finer lattices with physical values of the quark masses. We also should stress that current estimates for the bare lattice parameters that correspond to physical values of the light quark mass, $\hat{m}_q \simeq 0.04\hat{m}_s$, of course, are based on studies of the spectrum on lattices with finite cutoff. Eliminating these systematic effects will require further calculations on finer lattices. This may also improve the comparison with model calculations of the equation of state in the low temperature phase of QCD.

ACKNOWLEDGMENTS

This work has been supported in part by Contracts No. DE-AC02-98CH10886 and No. DE-FG02-92ER40699 with the U.S. Department of Energy, the Helmholtz Gesellschaft under Grant No. VI-VH-041, the Gesellschaft für Schwerionenforschung under Grant No. BILAER and the Deutsche Forschungsgemeinschaft under Grant No. GRK 881. Numerical simulations have been performed on the QCDOC computer of the RIKEN-BNL research center, the DOE funded QCDOC at BNL, the apeNEXT at Bielefeld University and the new BlueGene/L at the New York Center for Computational Science (NYCCS). We thank the latter for generous support during the burn-in period of NYBlue.

[1] J. I. Kapusta, Nucl. Phys. **B148**, 461 (1979).
[2] C. X. Zhai and B. M. Kastening, Phys. Rev. D **52**, 7232 (1995).
[3] P. Arnold and C. x. Zhai, Phys. Rev. D **51**, 1906 (1995).
[4] A. Vuorinen, Phys. Rev. D **68**, 054017 (2003).
[5] K. Kajantie, M. Laine, K. Rummukainen, and Y. Schroder, Phys. Rev. D **67**, 105008 (2003); F. Di Renzo, M. Laine, V. Miccio, Y. Schroder, and C. Torrero, J. High Energy Phys. 07 (2006) 026.
[6] P. Braun-Munzinger, K. Redlich, and J. Stachel, in *Quark Gluon Plasma 3*, edited by R. C. Hwa and Xin-Nian Wang (World Scientific Publishing, Singapore, 2004).
[7] C. W. Bernard *et al.* (MILC Collaboration), Phys. Rev. D **55**, 6861 (1997).
[8] A. Ali Khan *et al.* (CP-PACS Collaboration), Phys. Rev. D **64**, 074510 (2001).
[9] G. Boyd, J. Engels, F. Karsch, E. Laermann, C. Legeland, M. Lutgemeier, and B. Petersson, Nucl. Phys. **B469**, 419 (1996).
[10] F. Karsch, E. Laermann, and A. Peikert, Phys. Lett. B **478**, 447 (2000).
[11] C. Bernard *et al.*, Phys. Rev. D **75**, 094505 (2007).
[12] Y. Aoki, Z. Fodor, S. D. Katz, and K. K. Szabo, J. High Energy Phys. 01 (2006) 089.
[13] T. Blum *et al.*, Phys. Rev. D **55**, R1133 (1997).
[14] U. M. Heller, F. Karsch, and B. Sturm, Phys. Rev. D **60**, 114502 (1999).
[15] J. P. Blaizot, E. Iancu, and A. Rebhan, Phys. Lett. B **470**, 181 (1999); Phys. Rev. D **63**, 065003 (2001).
[16] J. O. Andersen, E. Braaten, E. Petitgirard, and M. Strickland, Phys. Rev. D **66**, 085016 (2002).
[17] M. Bluhm, B. Kampfer, R. Schulze, D. Seipt, and U. Heinz, Phys. Rev. C **76**, 034901 (2007).
[18] M. Cheng *et al.*, Phys. Rev. D **74**, 054507 (2006).
[19] S. R. Sharpe, Proc. Sci., LAT2006 (2006) 022.
[20] M. Creutz, Proc. Sci., LAT2006 (2006) 208; Proc. Sci., Lattice 2007 (2007) 007.
[21] A. Kronfeld, Proc. Sci., Lattice 2007 (2007) 016.
[22] I. Horváth, A. D. Kennedy, and S. Sint, Nucl. Phys. B, Proc. Suppl. **73**, 834 (1999); M. A. Clark, A. D. Kennedy, and Z. Sroczynski, Nucl. Phys. B, Proc. Suppl. **140**, 835 (2005).
[23] M. Cheng *et al.*, Phys. Rev. D **75**, 034506 (2007).
[24] J. Gasser and H. Leutwyler, Phys. Rep. **87**, 77 (1982).
[25] C. Bernard *et al.*, Phys. Rev. D **64**, 054506 (2001).
[26] A. Gray *et al.*, Phys. Rev. D **72**, 094507 (2005).
[27] C. T. H. Davies *et al.*, Phys. Rev. Lett. **92**, 022001 (2004).
[28] T. Ishikawa *et al.*, Proc. Sci., LAT2006 (2006) 181.
[29] C. Aubin *et al.*, Phys. Rev. D **70**, 094505 (2004).
[30] A. Andronic, P. Braun-Munzinger, and J. Stachel, Nucl. Phys. **A772**, 167 (2006).
[31] F. Karsch, K. Redlich, and A. Tawfik, Eur. Phys. J. C **29**, 549 (2003).
[32] C. M. Hung and E. Shuryak, Phys. Rev. Lett. **75**, 4003 (1995).
[33] R. D. Pisarski, Prog. Theor. Phys. Suppl. **168**, 276 (2007).

[34] E. Megias, E. Ruiz Arriola, and L. L. Salcedo, Phys. Rev. D **75**, 105019 (2007).
[35] S. Ejiri, F. Karsch, E. Laermann, and C. Schmidt, Phys. Rev. D **73**, 054506 (2006).
[36] O. Kaczmarek, F. Karsch, P. Petreczky, and F. Zantow, Phys. Lett. B **543**, 41 (2002); O. Kaczmarek and F. Zantow, Phys. Rev. D **71**, 114510 (2005); P. Petreczky and K. Petrov, Phys. Rev. D **70**, 054503 (2004).
[37] Y. Aoki, Z. Fodor, S. D. Katz, and K. K. Szabo, Phys. Lett. B **643**, 46 (2006).
[38] M. Laine and Y. Schroder, Phys. Rev. D **73**, 085009 (2006).
[39] M. Cheng (RBC-Bielefeld Collaboration), Proc. Sci., Lattice 2007 (2007) 173.
[40] F. Karsch, Proc. Sci. CPOD07 (2007) 026; C. DeTar and R. Gupta, Proc. Sci. Lattice 2007 (2007) 179.
[41] C. Bernard *et al.* (MILC Collaboration), Phys. Rev. D **71**, 034504 (2005).
[42] V. G. Bornyakov, S. M. Morozov, Y. Nakamura, M. I. Polikarpov, G. Schierholz, and T. Suzuki, Proc. Sci. Lattice 2007 (2007) 171.